INSTITUTO SUPERIOR TÉCNICO
Universidade Técnica de Lisboa

HIV-1 Infection Model Analysis and Therapy Design using a Nonlinear Control approach

João Gonçalo Silva Marques
(Licenciado)

Dissertação para obter o grau de Mestre em

Engenharia Biomédica

Júri

Presidente:	Professor Doutor Paulo Jorge Peixeiro de Freitas
Orientador:	Professor Doutor João Manuel Lage de Miranda Lemos
Co-Orientador:	Professora Doutora Emília de Jesus da Encarnação Valadas
Acompanhante:	Professora Doutora Susana de Almeida Mendes Vinga Martins

October 17, 2011

Anyone who has never made a mistake has never tried anything new.

Albert Einstein

Acknowledgments

First of all, I would like to thank Prof. João Miranda Lemos, for the opportunity of joining an European project of this importance, and for all the guidance and support he always showed to me. I would also like to thank Prof. Susana Vinga, for all the invaluable advices and comments throughout this work, and for always being available when I needed something. To the KDBIO group, and especially to my colleagues at room 128, thank you for all the support and good moments.

I also want to thank Prof. Emília Valdas and Ana Filipa Sutre, who were always available to meet me at 8 a.m., even if only for a brief discussion at times I couldn't even understand my own results. Also, for the priceless comments on the details for the clinical part of my work, thank you.

To Ricardo Aires, I would like to thank you for the advices throughout this work, and, almost as important, for the thesis template, without which I would still be working around with LaTeX.

To Miguel Amador, for always being there to cheer me up, even when everything else did not seem to work. Your friendship over the past 5 years has been inestimable, and I only wish to cherish it even further. Thank you.

To Joana Nunes, a big thank you for your comprehension and support throughout this journey. Even when things did not look that good, you always had a positive word for me. For all of the endless times on the Internet when we should be working, a big thank you! It would not have been possible without you.

Finally, to my family. To my father, for asking how my thesis is going everyday, and what am I working on after all. To my mother, for all of the times I missed dinner without warning, and also for the times when my mood was not the best. To my sister, for helping whenever she could. This dissertation quote is on her. To my brother, for being my brother, and for always having a completely irrelevant but still interesting breaking news about football or video games.

This work was supported by FCT under the project *HIVCONTROL - Control based on dynamic modeling of HIV-1 infection for therapy design*, contract PTDC/EEA-CRO/100128/2008, and INESC-ID multiannual funding through the PIDDAC Program funds.

FCT Fundação para a Ciência e a Tecnologia
MINISTÉRIO DA EDUCAÇÃO E CIÊNCIA

Abstract

There is currently an increasing interest in the study of Human Immunodeficiency Virus 1 (HIV-1) infection dynamics, with several mathematical models developed with this objective. In some of them, there is the attempt of considering the action of antiretroviral drugs. However, in most cases, the concern is only in the relation between drug effect and viral load. In addition, the drug effect is usually seen as a continuous variable. In order to bring the analysis of HIV-1 dynamic models closer to the reality, this work deals with drug doses instead of drug effects, which are administered to patients in the form of a series of discrete events. These drug doses are then processed by a Pharmacokinetic (PK) and Pharmacodynamic (PD) model, in order to compute drug effect from the doses administered to the patient. Moreover, an adherence and virus resistance model is also included, so that their impact can be analyzed in simulations, since they play an important role in real patients. After this analysis, a sensitivity and local identifiability analysis is performed for the proposed model, and it is concluded that there are time periods, especially in early stages of the infection, that are far more informative than others, which may help in the planning of measurements. In addition, it is seen that the model is not identifiable, and a subset of unidentifiable parameters is obtained. Different therapy combinations are used to test the developed model, and it shown that the outcome of a regular therapy, but with patient adherence of 50%, is far better than that of a therapy with 100% patient adherence, but with drug doses being administered with half the frequency. Finally, using a nonlinear control approach, it is also demonstrated that it is possible to achieve an undetectable viral load with drug doses far below those currently used in practice. However, the developed algorithm does not take into account resistance development, which may lead the therapy predicted by the controller to eventually fail.

Keywords

Human Immunodeficiency Virus 1, Infection Dynamic Models, Antiretroviral Drugs, Pharmacokinetics/Pharmacodynamics, Sensitivity and Identifiability Analysis, Control Theory.

Resumo

O Vírus da Imunodeficiência Humana 1 (VIH-1) tem sido alvo de um crescente interesse por parte da comunidade científica, com o desenvolvimento de vários modelos matemáticos. Em alguns, existe a preocupação de incluir a acção de fármacos antiretrovíricos, sendo que, na maior parte dos casos, o interesse fica apenas pela relação entre o efeito dos fármacos e a evolução da carga viral, sendo este normalmente visto como uma variável contínua no tempo. Para aproximar este tipo de análises da realidade, este trabalho lida com doses de fármacos directamente, sob a forma de eventos discretos (que pretendem simular a toma de comprimidos). Estas doses são depois processadas por um modelo de farmacocinética e farmacodinâmica, para se calcular o seu efeito com base na dose administrada. Inclui-se também um modelo de aderência e de resistência do vírus à terapêutica, já que estes efeitos têm grande importância em casos reais. Faz-se também uma análise de sensibilidade e identificabilidade local para o modelo proposto, e conclui-se que existem períodos, no início da infecção, muito mais informativos que outros, o que pode auxiliar no planeamento de análises e ensaios clínicos. Mostra-se ainda que o modelo é não identificável, e um conjunto de parâmetros não identificáveis é obtido. Diferentes combinações de terapêuticas são utilizadas para testar o modelo proposto, e mostra-se que o resultado para uma terapêutica em que há uma aderência do paciente de 50%, é muito superior ao resultado para uma terapia com 100% de aderência, mas com as doses de fármaco administradas com metade da frequência. Finalmente, utilizando uma abordagem de controlo não linear, demonstra-se ainda que é possível obter cargas virais indetectáveis com doses de fármacos muito inferiores às que são prescritas actualmente. Contudo, o algoritmo desenvolvido não tem em consideração o desenvolvimento de resistência às drogas, o que pode levar a uma eventual falha da terapêutica prescrita pelo controlador.

Palavras Chave

Vírus da Imunodeficiência 1, Modelos de Infecção Dinâmica, Fármacos Antiretrovíricos, Farmacocinética/Farmacodinâmica, Análise de Sensibilidade e Identificabilidade, Teoria de Controlo.

Contents

List of Figures

List of Tables

Abbreviations

3TC Lamivudine

AIDS Acquired Immune Deficiency Syndrome

CCR5 C-C Chemokine Receptor type 5

CD4 Cluster of Differentiation 4

CXCR4 C-X-C Chemokine Receptor type 4

DNA Deoxyribonucleic Acid

HAART Highly Active Antiretroviral Therapy

HIV-1 Human Immunodeficiency Virus 1

IDV Indinavir

LTR Long Terminal Repeat

mRNA Messenger Ribonucleic Acid

NNRTI non-Nucleoside Reverse Transcriptase Inhibitor

NRTI Nucleoside analog Reverse Transcriptase Inhibitor

NtRTI Nucleotide analog Reverse Transcriptase Inhibitor

PD Pharmacodynamic

PI Protease Inhibitor

PK Pharmacokinetic

RLS Recursive Least Squares

RNA Ribonucleic Acid

RT reverse transcriptase

RTI Reverse Transcriptase Inhibitor

SVD Singular Value Decomposition

List of Symbols

D_1	RTI drug dose for PK model	12
D_2	PI drug dose for PK model	12
D_1^A	RTI drug dose that the patient actually takes	12
D_2^A	PI drug dose that the patient actually takes	12
C_{P1}	RTI plasma concentration	12
C_{P2}	PI plasma concentration	12
u_1	RTI drug effect	12
u_2	PI drug effect	12
a_{ij}	PK model coefficients	13
$E_{\max}$	Maximum Drug Effect	13
C_{50}	Drug plasma concentration that corresponds to half the maximum drug effect	13
A	Patient Adherence Value	14
$C_{50_{base}}$	C_{50} base value in the resistance model	14
$f_R(t)$	Drug resistance factor	14
L_R	Drug concentration limit for resistance development	14
K_R	Drug resistance development rate	14
T	Healthy CD4+ T cell population	15
T^*	Infected CD4+ T cell population	15
ν	HIV-1 Virus population	15
s	Production rate of healthy CD4+ T cells from the thymus	15
d	Average per capita death rate of healthy CD4+ T cells	15
β	Healthy CD4+ T cell infection rate coefficient	15
μ	Average per capita death rate of infected CD4+ T cells	15
k	Average per capita virus production rate	15
c	Average per capita clearance rate of free virus particles	15
$\boldsymbol{\theta}$	HIV-1 dynamic model parameter vector	16
$\mathbf{X}$	HIV-1 dynamic model state vector	16
$\mathbf{f}$	Dynamic model of HIV-1 infection mode	16
R_0	HIV-1 basic reproductive ratio	17

$\overline{\mathbf{X}}^1$	HIV-1 infection model healthy equilibrium point	17
$\overline{\mathbf{X}}^2$	HIV-1 infection model endemic equilibrium point	17
$\mathbf{X}_0$	HIV-1 dynamic model state initial conditions	17
L	Latently infected CD4+ T cell population	22
p	average per capita growth rate of healthy CD4+ T cells	22
$T_{\max}$	maximum CD4+ cell count	22
β_L	average per capita activation rate of latently infected CD4+ T cells	22
β'	infection rate coefficient (same as β)	22
M	Healthy CD4+ macrophage population	23
M^*	Infected macrophage population	23
s_M	Healthy CD4+ macrophages replenishment rate	23
d_M	Average per capita death rate of healthy CD4+ macrophages	23
β_M	CD4+ macrophages infection rate coefficient	23
μ_M	Average per capita death rate of infected CD4+ macrophages	23
k_M	Average per capita virus production rate from CD4+ macrophages	23
$\mathbf{S}_p$	Sensitivity matrix with respect to parameter p	28
$\mathbf{S}$	Sensitivity Tensor	28
$\mathbf{S}^m$	Sensitivity Tensor rearranged as a matrix	29
$\mathbf{R}$	Sensitivity correlation matrix	31
$\rho(P,Q)$	Pearson's correlation coefficient between P and Q	31
$\mathbf{U}^m$	$\mathbf{S}^m\mathbf{S}^{m\mathrm{T}}$ matrix of eigenvectors	33
$\mathbf{V}^m$	$\mathbf{S}^{m\mathrm{T}}\mathbf{S}^m$ matrix of eigenvectors	33
Σ^m	Square root of $\mathbf{S}^{m\mathrm{T}}\mathbf{S}^m$ matrix of eigenvalues	33
$\mathbf{A}_{3\mathrm{TC}}$	Optimized parameters for the lamivudine PK model	39
$\mathbf{A}_{\mathrm{IDV}}$	Optimized parameters for the indinavir PK model	39
J	Nonlinear control cost function	51

1

Introduction

Contents

1.1 Motivation

Acquired Immune Deficiency Syndrome (AIDS) is a disease caused by Human Immunodeficiency Virus 1 (HIV-1) that affects the human immune system, reducing its effectiveness and leaving it susceptible to other diseases (called opportunistic diseases). It was first reported in June 5 1981, and it is believed to have been passed into the human population by chimpanzees around 1900 in west-central Africa [1].

HIV-1 is a retrovirus that targets preferentially CD4+ T cells, that are responsible for helping other white cells in the immune response. This cell pool can have very low counts, caused either by viral killing (due to the accumulation of virus particles inside the cell) or by elimination from the organism (due to apoptosis or immune system recognition). When the CD4+ T cell count is below than 200 cell/mm^3, the patient is said to have developed AIDS [2]. The infection by HIV-1 normally comprises three stages: *acute* infection, *chronic* infection, and *symptomatic* infection or AIDS, as it is shown in Figure 1.1.

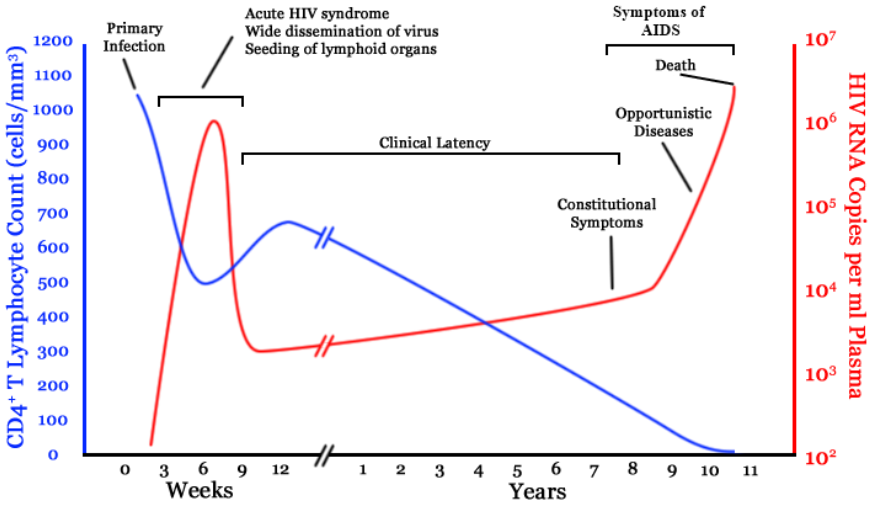

Figure 1.1: Generalized evolution of untreated HIV-1 infection. Based on [3].

Statistics show that, during 2009 only, about 2.6 million people were newly infected with HIV-1, and that there were around 1.8 million HIV-1 related deaths. When compared to the figures of 2001 (3.1 million newly infected people), it is possible to conclude that there are now less new HIV-1 cases than 10 years ago [4]. However, no cure has yet been found for HIV-1 infection, and there are as many as 33.3 million people living with HIV-1, which corresponds to about 0.5% of the world population. The largest fraction of this number refers to Sub-Saharan Africa (67.5%), where the prevalence of the infection is, in average, 5%. In Figure 1.2 is represented the distribution of HIV-1 infection prevalence worldwide.

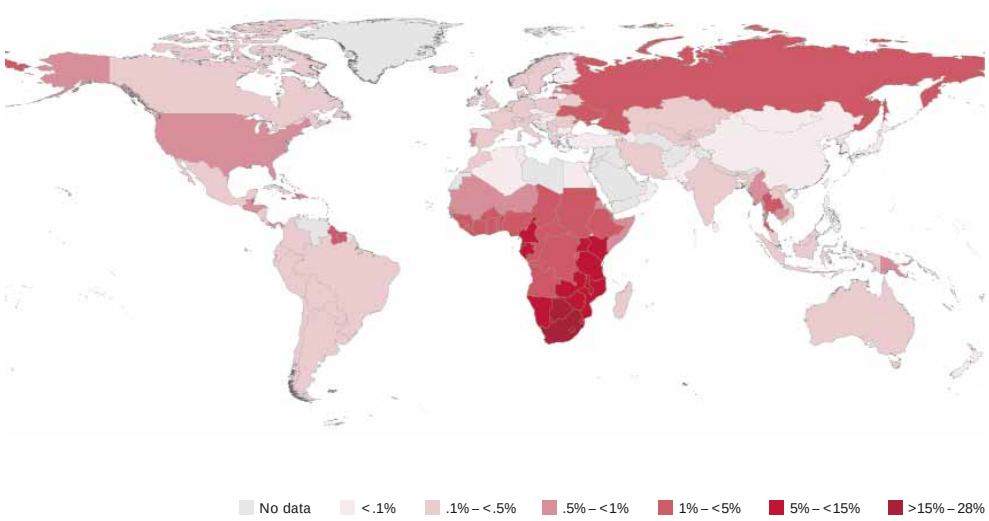

Figure 1.2: Global prevalence of HIV-1 infection in 2009. Data from [4].

As it is possible to see, Sub-Saharan African countries have the highest prevalence of HIV-1 infection. These underdeveloped countries often lack efficient and affordable access to antiretroviral therapy, shortening the average life expectancy for an infected patient.

Nowadays, HIV-1 infection is treated with Highly Active Antiretroviral Therapy (HAART), which uses a combination of several antiretroviral drugs (mainly Reverse Transcriptase Inhibitors (RTIs) and Protease Inhibitors (PIs)), and the improvement in the life expectancy and quality of infected people is considerable [5]. The reason why combinations of multiple drugs are used is to prevent the appearance of viral resistance to the therapy, which can lead to its failure. Moreover, for preventing the appearance of AIDS, patients need to follow the therapy rigidly. In these conditions, HAART may extend an infected patient's life for several years.

However, there are some drawbacks in the efficacy of HAART. Causes such as low availability of antiretroviral drugs (either because they are scarce or not affordable) or appearance of side-effects can lead to the interruption of the therapy, compromising its success. When patient adherence is low, or when patient interrupts therapy, the virus has the opportunity to mutate and develop strains that are resistant to antiretroviral drugs, rendering them useless.

These problems associated with HAART, together with the high costs involved in this kind of therapy, have led the scientific community into the development and analysis of mathematical models that can mimic HIV-1 infection features, in the attempt of better understanding the infection dynamics. Some of these models also incorporate a way of reproducing drug effects, and their impact in the infection dynamic system. However, most models that consider drug action are often only concerned with drug efficacy, and do not consider that medication is taken a discrete event that need to be converted into a continuous drug efficacy. This work has the objective of studying some of these methods, and incorporating into one of them the action of RTIs and PIs, making use of their pharmacokinetic and pharmacodynamic properties, in order to allow the sim-

ulation of discrete drug doses. Furthermore, the patient adherence situation is also addressed, and a resistance model is proposed and simulated.

One challenge that still remains is not only that of estimating the model parameters using real patient data, but even being able to state whether the model parameters may be identified if experimental data is available. This topic is addressed in this work, by means of a sensitivity analysis to the model parameters, and a subsequent identifiability analysis.

Once the dynamic modeling is achieved, the next natural step is to understand if it is possible to use an automatic control on the models. This may prove to be a powerful tool in therapy design, that can be adapted to each patient, rather than having all the patients following the same prescriptions. If this is possible, it may allow to decrease the drug doses that are given to the patients, reducing cost and side-effects.

1.2 State of The Art

Mathematical Biology was founded by Fisher, Haldane and Wright in the first half of the 20^{th} century, with their work on Darwin's theory of evolution, where their mathematical models show how mutation and selection work together to govern evolution. However, others had already shown that this was a promising field, such as Mendel (with his statistical interest in biology that led to the foundations of genetics in the 19^{th} century), Volterra (with Lotka-Volterra equations early in the 20^{th} century), or even Bernoulli (that studied the effectiveness of variolation techniques against small pox with mathematical models in the 18^{th} century) [6].

The application of mathematical models to HIV-1 infection analysis was greatly boosted by Nelson and Perelson, starting with the paper by Perelson *et al* [7], where a dynamic HIV-1 infection model is analyzed and discussed. Apart from this one, other models for the HIV-1 infection were developed, both stochastic [8–10] and deterministic [11–14]. These papers showed that there are events that take place in a time scale of days and weeks, that had not yet been observed since they are fast when compared to the time scale of AIDS. However, there was always a focus in incorporating other characteristics in these models. More complex models began to appear, some considering different cell populations [15–17], others including pharmacokinetic and pharmacodynamic effects [15, 18], and even others including patient adherence and drug resistance [19].

Another issue that has been given relevance is parameter estimation. Approaches in [20–22] propose methods for estimating parameters from clinical data. Other papers are more concerned with the issue of identifiability, and methods for assessing this property in the case of AIDS are proposed in [23–25].

The development of dynamic models that are able to mimic the dynamics of HIV-1 infection allowed for the development of therapy design techniques, using control approaches [26]. In the particular case of the HIV-1 infection, nonlinear control techniques play an important role [27, 28] and have been the subject of great development. These algorithms are able to drive the viral load

below pre-determined thresholds, receiving input from clinical data. The combination of control theory with HIV-1 dynamic models allows to obtain the optimal therapy that keeps the viral load undetected.

1.3 Original Contributions

This dissertation contributions begin with a characterization of several HIV-1 dynamic models, and a comparative study of these models. Moreover, a pharmacokinetic/pharmacodynamic model is described and characterized, as a way of being incorporated into the infection model. A full description of the adherence and drug resistance models used in this work is also provided. For one of the models approached, a sensitivity and identifiability study is performed, as a way of knowing whether the model parameters are identifiable from clinical data or not. Finally, a controller is also implemented, which, coupled to the full HIV-1 dynamic model, is able to drive the viral load to undetectable values.

The work developed in this dissertation also contributed to the following publication:

- J. G. Marques, S. Vinga and J. M. Lemos. Local Identifiability of a HIV-1 infection model using a sensitivity approach, in Proceedings of the Eigth International Workshop on Computational Systems Biology, Zurich, pages 136-139, June 2011.

This work also resulted in an oral communication with the title Simulação dinâmica da infecção por VIH-1, com incorporação de fármacos, adesão, e resistência à terapêutica, 12º Encontro Nacional de Actualização em Infecciologia, Porto, October 2011.

1.4 Thesis Outline

This dissertation starts with a full description on the HIV-1 infection model in Chapter 2. First, the anatomy and pathophysiology of the viral infection is described. After that, the mathematical model is explained in detail, according to the physiological aspects approached. Finally, a general comparative study with other dynamic models is done.

In Chapter 3, a local sensitivity and identifiability analysis is performed, allowing to assess whether the model parameters are identifiable or not.

After that, the pharmacokinetic and pharmacodynamic models for some of the most used antiretroviral drugs are further detailed in Chapter 4. Furthermore, simulations of the full model (including the dynamic model, antiretroviral drugs, patient adherence and drug resistance) are performed for multiple situations, and results are compared and discussed.

Finally, in Chapter 5, a control approach is developed to address the challenge of building a personalized therapy that reacts to the patient response to the treatment. Two algorithms are developed in this Chapter: one that considers only the effect of antiretroviral drugs, and another

that allows to use drug doses as inputs, and then computes the efficacies based on these inputs. Results from both algorithms are compared and discussed.

2

HIV-1 Infection Model

Contents

This chapter focuses on a full description of the HIV-1 infection model used throughout this work. First, the HIV-1 anatomy and pathophysiology are described. After that, the two types of antiretroviral drugs are presented. In the subsequent sections, the infection mechanism is translated into a mathematical model, including drug effects, patient adherence, and virus resistance development.

2.1 Pathogenesis of HIV-1 Infection

2.1.1 HIV-1 Morphologic Structure and Genome

The Human Immunodeficiency Virus 1 (HIV-1) is a retrovirus that belongs to the family of lentiviruses, a family of viruses characterized by its long incubation time. HIV-1 viral particles have a diameter of approximately 100 nm, and are roughly spherical. Each particle contains two copies of a 9749 nucleotides long single-stranded RNA, surrounded by a conical capsid of viral protein (p24). This capsid is enclosed by a protein matrix (p17), which in turn is anchored to the inside of the viral lipoprotein membrane. The virus membrane contains 72 glycoprotein complexes, each composed of trimers of an external glycoprotein (gp120) and a transmembrane spanning protein (gp41). However, during the process of budding, the virus may incorporate host proteins from the host cell membranes into its own lipoprotein layer that may facilitate adhesion to other target cells. Each viral particle contains all the enzymes that are necessary for replication inside a host cell: a protease, an integrase, and a reverse transcriptase (RT) [6].

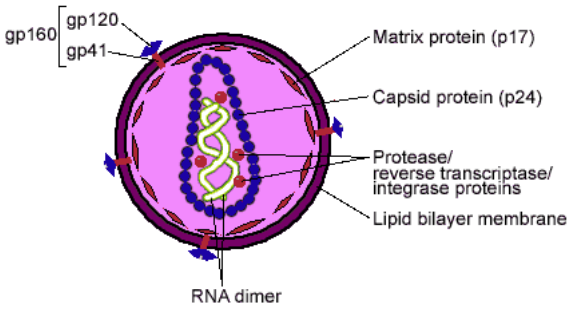

Figure 2.1: Structure of a HIV-1 viral particle. In [29].

The typical replication competent retroviruses depend on three genes: *gag* ("group-antigen"), *pol* ("polimerase") and *env* ("envelope"). The classical structure of a retroviral genome is 5' LTR-*gag*-*pol*-*env*-LTR 3'. The Long Terminal Repeat (LTR) regions represent the two end parts of the viral genome, where the connection with the host cellular DNA is made. Therefore, these regions do not encode for any viral proteins. The *gag* and *env* genes code for the nucleocapsid and the glycoproteins of the viral membrane, whereas the *pol* gene codes for the viral enzymes. HIV-1 follows this general structure, but contains six other genes that contribute to its genetic complexity.

These genes have been classified as accessory genes since they are not absolutely required for the virus replication *in vitro*. However, further studies show that they code for regulatory proteins, transcriptional activators and nuclear export factors, among others [6].

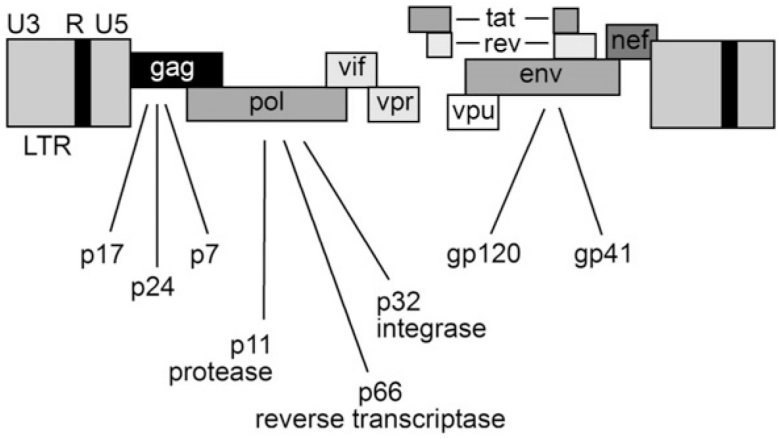

Figure 2.2: HIV-1 genome structure. In [6].

2.1.2 HIV-1 Replication Cycle

HIV-1 replication cycle can be divided in three main stages: the *infection* stage, in which the virus particle enters the host cell by fusing its envelope with the host membrane; the *replication* and *transcription* stage, where the virus proteins are produced using the cellular machinery; and the *assembly* stage, in which new virus particles are formed and released into the blood stream.

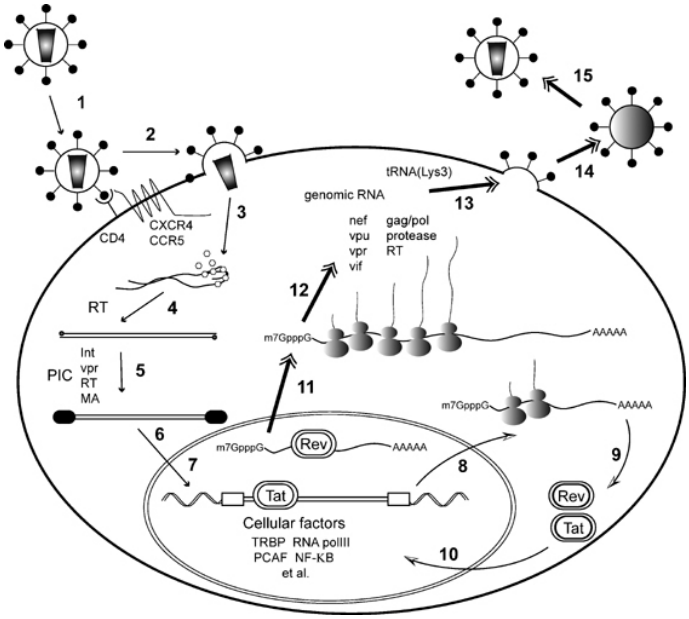

Figure 2.3: HIV-1 replication cycle [30]. For further details on each step, see text below.

The entry of the virus into the host involves complex interactions between the virus membrane and specific receptors on the host cell (CD4 and a chemokine, which is generally CCR5 or CXCR4).

In free virus particles, the gp41 structure is stabilized by interactions with gp120. When gp120 binds to CD4 and a chemokine receptor (step 1), a conformational change occurs in gp120 that alters gp120-gp41 interactions. This perturbation triggers gp41 to, among other changes, insert itself into the target membrane (step 2), allowing the virus to pour its contents into the cell (step 3) [31].

The conversion of RNA into proviral DNA (mediated by the RT) occurs in the cytoplasm of the host cell (step 4). This process is error-prone, and mutations that occur here are a possible source of drug resistance. After this, the viral DNA migrates to the nucleus (steps 5 and 6) and it is integrated into a host chromosome with the help of integrase (step 7). During the replication process (through which RNA is formed from DNA), the integrated viral DNA is transcribed into mRNA. This mRNA is retained in the nucleus until it undergoes splicing. However, the first viral proteins translated from spliced mRNA (steps 8 and 9) bind to viral mRNA (step 10), allowing the unspliced mRNA to exit the nucleus (step 11). The translation of the whole mRNA results in the production of the structural proteins needed to encapsulate the virus genetic material into new virus particles (step 12) [6].

The assembly stage starts when the gp41 and gp120 glycoproteins reach the cell membrane. Here, the gp120 is anchored to the membrane by gp41. Other virus proteins (Gag and Gag-Pol) and the virus genetic material become connected to the plasma membrane as the new virus particle takes shape (step 13). After the new particle is complete, it still needs to undergo a maturation stage, during which viral proteins are cleaved into individual functional proteins and enzymes (step 14). After the maturation is complete, the virus is able to infect another cell (step 15) [30, 32].

2.1.3 Antiretroviral Drugs

Antiretroviral drugs are, by definition, a class of medication that is used specifically for retroviral infections. They belong to a broader group of drugs named antimicrobials, and are almost harmless to the host, targeting only the virus [33]. In the case of HIV-1, there are two main types of antiretroviral drugs: RTIs and PIs[1].

RTIs operate at the level of RT inhibition, preventing the viral RNA from being converted into DNA. This means that, even though the viral contents are injected into the host cell, there is never an actual infection, since the viral genetic material is never incorporated into the cell genome. There are three types of RTIs: Nucleoside analog Reverse Transcriptase Inhibitors (NRTIs), Nucleotide analog Reverse Transcriptase Inhibitors (NtRTIs), and non-Nucleoside Reverse Transcriptase Inhibitors (NNRTIs). NRTIs and NtRTIs are the analogues of deoxynucleotides that occur naturally, and that are needed to synthesize viral DNA. Therefore, these inhibitors compete with the natural nucleotides for being incorporated into the viral DNA chain. However, these inhibitors do not have a 3'-hydroxyl group that is essential for the next nucleotide to bond, meaning that the

[1]There has been development in two other drug classes (Entry inhibitors and Integrase Inhibitors), but these are not commonly used yet, and therefore their description is left out of this work.

process of DNA synthesis is stopped. These two inhibitors are classified as competitive. NNRTIs, on the other hand, bind to the RT enzyme on a different location than NRTIs and NtRTIs, and are not incorporated in the DNA synthesis process. Their purpose is to non-competitively inhibit the movement of specific domains that are crucial for the synthesis process to be successful. Therefore, they are classified as non-competitive. Comercially available examples of RTIs are: zidovudine, lamivudine, abacavir (NRTIs), tenofovir (NtRTIs), efavirenz and nevirapine (NNRTIs) [6]. For a complete list of RTIs, please refer to Appendix A.

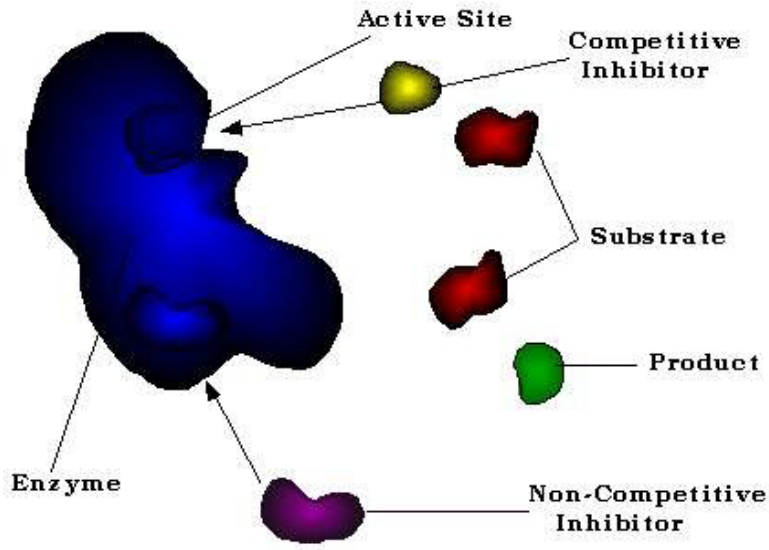

Figure 2.4: Competitive and non-competitive inhibition. For further detail, see text above.

PIs, unlike RTIs, act after the cell has been infected and the virus genome has been incorporated into a host chromosome. Their main objective is to prevent a correct assembly of new virions, through the inhibition of viral proteases. If these enzymes are not active, then the viruses cannot cleave their proteins, and new virus particles cannot be assembled. Examples of this class of inhibitors are saquinavir, ritonavir and indinavir [6]. For a complete list of PIs, please refer to Appendix A.

2.2 Model General Description

The HIV-1 infection model considered in this work allows to describe the infection dynamics (CD4+ T cell count and virus load), taking into account specific initial conditions, as well as the drug doses that the patient takes. The given model has four main blocks: the adherence model, the Pharmacokinetic (PK) model, the Pharmacodynamic (PD) model, and the virus dynamics. The model is summarized in Figure 2.5.

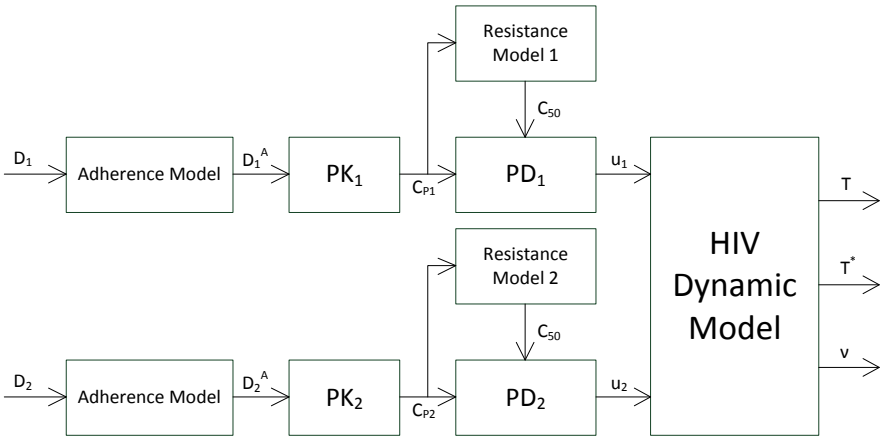

Figure 2.5: General HIV-1 infection model, including PK+PD, adherence and resistance.

In Figure 2.5, D_1 and D_2 represent the RTI and PI doses, respectively. These two inputs allow to simulate the treatment of HIV-1 infection. A simplification is made here, since real patients take more than one drug of each kind, to minimize resistance development.

The drug inputs D_i then go through an Adherence Model, which transforms these inputs according to whether the patients follows the prescription or not. Therefore, some of the doses might not be taken by the patient, meaning that they have no effect on the actual model dynamics. The drug doses that are actually taken by the patient are represented by D_1^A and D_2^A.

After pre-processing the drug inputs, it is necessary to convert these doses into drug effect, which will range from 0 to 1. For this, a PK+PD model is considered. The first converts the input into drug plasma concentration over time (C_{P1} and C_{P2}), while the second takes this concentration and outputs the drug effect (u_1 and u_2). It is also considered that virus resistance may develop, which will result in lower drug effects.

Finally, the drug effects serve as input for the HIV-1 dynamic model that allows the infection simulation.

2.3 Pharmacokinetic and Pharmacodynamic Models

2.3.1 Pharmacokinetic Model

Pharmacokinetics (PKs) is the study of the concentration of drugs in tissues as a function of time, and eventually dose schedule [34]. These models are almost certain to be different from drug to drug, and therefore it is necessary to find a model for each considered drug. Since there are two drugs being studied in this work, two PK models are needed. In this work, a two-compartment system is used for each PK model [34]. This system is summarized in Figure 2.6.

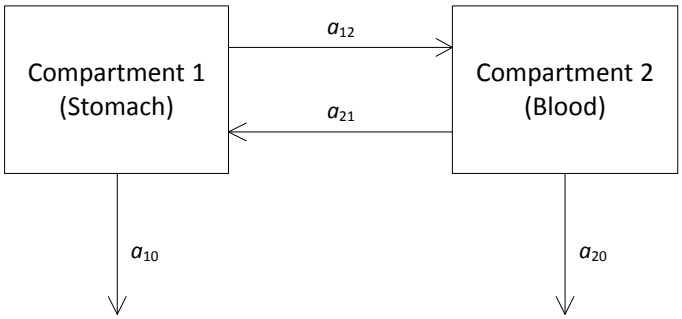

Figure 2.6: Two-compartment model used to represent the HIV-1 infection PK model.

The model described in Figure 2.6 can also be represented as

$$\dot{\mathbf{x}}(t) = \mathbf{A}\mathbf{x}(t),\ \mathbf{x}(0) = \mathbf{x}_0,\ t \geq 0 \tag{2.1}$$

where

$$\mathbf{A} = \begin{bmatrix} -(a_{12} + a_{10}) & a_{21} \\ a_{12} & -(a_{21} + a_{20}) \end{bmatrix},\ \mathbf{x} = \begin{bmatrix} x_1 \\ x_2 \end{bmatrix} \tag{2.2}$$

The constants a_{ij} in Figure 2.6 and (2.2) are specific for each drug, and are therefore said to be pharmacokinetic parameters of the drug. a_{21} and a_{12} are the nonnegative transfer coefficients form compartment 2 (x_2) to compartment 1 (x_1) and vice-versa, respectively. a_{11} and a_{22} are the nonnegative rates at which the drug is eliminated from compartment 1 and compartment 2, respectively. Most compartmental models consider $a_{10} = 0$, as a way of expressing that the elimination process happens only in the main compartment. That is reasonable in many cases (as the brain, or the liver), where the only way of eliminating substances is through the blood stream. However, if the stomach is seen as one compartment, then it only makes sense that $a_{10} \neq 0$, since not all drug must be absorbed into the blood. There may be a significant amount of drug that follows the gastrointestinal tract and is eventually eliminated from the body.

2.3.2 Pharmacodynamic Model

Pharmacodynamics (PDs) is the study of the relationship between drug concentration and drug effect [34]. It is assumed that the drug effect is proportional to the drug concentration, but in a non-linear way. This happens because there is the need of restraining the drug effects to values between 0 and 1. In this work, the PD model is given by the Hill equation

$$u(C_P) = E_{\max}\frac{C_P}{C_P + C_{50}} \tag{2.3}$$

where E represents the drug effect, and is bounded between 0 and 1, $E_{\max}$ is the maximum drug effect, and C_{50} is the drug concentration that corresponds to half the maximum drug effect [34]. This value is said to be a pharmacodynamic parameter, and is specific for each drug. Therefore, there is one PD model for each drugs, meaning that two PD models are used in this work.

2.4 Adherence and Resistance Models

2.4.1 Adherence Model

The lack of patient adherence to a treatment regimen is one of the major causes for HIV-1 treatment failure. If the patient does not take the drug doses prescribed, this will have an impact on the system dynamics. Since this factor is present in a significant part of real HIV-1 infected patients, it is considered in this work. According to [35], adherence can be defined as

$$A = \begin{cases} 1, & \text{if all drug doses are taken by the patient} \\ R_k, & \text{if } 100R_k\% \text{ drug doses are taken by the patient.} \end{cases} \tag{2.4}$$

2.4.2 Drug Resistance Model

Drug resistance modeling intends to simulate the possible appearance of virus resistance to drug effects. In this work, it is considered that the virus may develop drug resistance if the drug plasma concentration falls below a certain threshold. If this happens, then an equal drug concentration has less effect than it had before. This effect is irreversible, meaning that resistance does not disappear, even if the drug concentration rises above the threshold again.

In terms of the model, this effect operates by changing the C_{50} value in the Hill equation. An increase in this parameter value means that, after resistance development, more drug will be necessary in order to achieve similar efficacy results. The parameter C_{50}, defined in Section 2.3.2, is now redefined as in [36].

$$C_{50}(t) = f_R(t) C_{50_{base}} \tag{2.5}$$

where $f_R(t)$ is given by

$$f_R(t) = 1 + K_R \int_0^t \max\left[0, L_R - C_P(\tau)\right] d\tau \tag{2.6}$$

Each time the drug concentration falls below L_R (a model parameter), f_R increases, and therefore C_{50} also increases. Moreover, this increase is irreversible, meaning that once resistance is acquired, it cannot be treated, even if the drug dose is adjusted. This model also depends on another parameter, K_R, that controls the integral gain, and that defines the resistance development rate [36].

2.5 HIV-1 Dynamic Model

2.5.1 CD4+ T Cell Dynamic Model

To generate a realistic model of T-cell infection by HIV-1, it is first necessary to consider the T cell population dynamics in the absence of the virus. T cells are produced in the bone marrow, and migrate to the thymus, where they become immunocompetent T cells [37]. Even though the

thymus suffers changes in volume and weight during a person's lifetime, it is assumed here that new healthy T cells are supplied by the thymus at a constant rate [7]. This is a good approximation, since the greatest changes in the thymus occur before adulthood, and only seldom patients are followed since before they are adults. However, in healthy individuals the number of T cells in the blood is kept at a relatively constant level, meaning that T cells are also eliminated from the body. This makes sense, since every cell in the human body as an average life span [37]. As a result, the T cell dynamic model in the absence of virus is given by

$$\dot{T} = s - dT \tag{2.7}$$

where T represents the CD4+ T cell population, s is the rate at which new healthy CD4+ T cells are released into the blood stream, and $1/d$ is the CD4+ T cells average life span. In this model, it is assumed that healthy CD4+ T cells do not proliferate. This is not true, but it is still a good approximation. In patients that may have had their thymus removed it would make sense to include this extra term, since there would not be healthy T cell replenishment otherwise.

2.5.2 HIV-1 Infection Dynamic Model

The HIV-1 infection model used in this work [12, 13, 38, 39] comprises 3 states: healthy CD4+ T cells (T), infected CD4+ T cells (T^*), and free virus particles (ν).

$$\begin{cases} \dot{T} &= s - dT - (1-u_1)\beta T\nu \\ \dot{T}^* &= (1-u_1)\beta T\nu - \mu T^* \\ \dot{\nu} &= (1-u_2)kT^* - c\nu \end{cases} \tag{2.8}$$

The first equation, that defines the healthy CD4+ T cell population dynamics in the presence of HIV-1, is very similar to that present in (2.7). s and d are defined as above, and the extra term reflects the possibility that an healthy cell may become infected, and it is modeled using a simple mass-action type of term, with a rate constante β. The result of infection gives rise to infected CD4+ T cells. These cells may have a different life span ($1/\mu$) than healthy cells, which means that, generally, $\mu \neq d$. Finally, free virus particles are produced by infected cells at an average per capita rate k, and have an average life span of $1/c$ [7, 15].

The drug action influences the model via u_1 and u_2 (see Section 2.2). The RTI action is modeled by u_1, while PI action is modeled by u_2. As it is explained in Section 2.1.3, RTIs prevent the viral RNA from being converted into DNA. When this drug is successful, the host cell is not infected. Therefore, the term $(1-u_1)$ affects the first and second state in (2.8). On the other hand, PIs prevent the correct assembly of virus particles. Consequently, if the drug is successful, the amount of virus produced by an infected cell is lower, and that is why the term $(1-u_2)$ affects the last state in (2.8).

The diagram in Figure 2.7 and the summarized parameter explanation in Table 2.1 allow for a better understanding of the system described in (2.8).

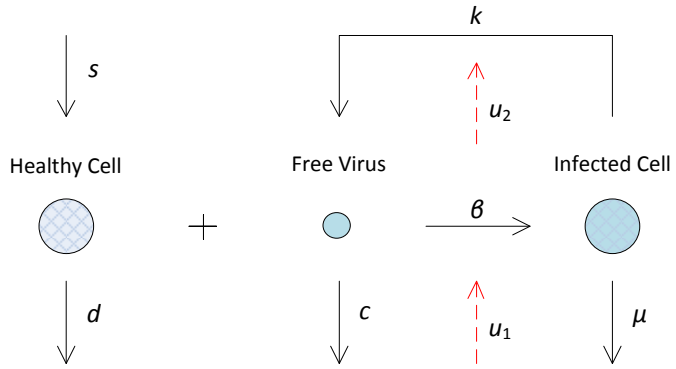

Figure 2.7: HIV-1 infection dynamic model. The red dashed arrows represent the drug inhibitory effect.

Table 2.1: Parameter description for the HIV-1 infection model in Figure 2.7. To be noted that units for T and T^* are measured in cell mm^{-3} and ν is measured in particle mm^{-3}.

Parameter	Description	Units
s	healthy CD4+ T cells replenishment rate	cell mm^{-3} day^{-1}
d	average per capita death rate of healthy CD4+ T cells	day^{-1}
β	infection rate coefficient	particle^{-1} mm^3 day^{-1}
μ	average per capita death rate of infected CD4+ T cells	day^{-1}
k	virus production rate coefficient	particle cell^{-1} day^{-1}
c	average per capita death rate of virus particles	day^{-1}
u_1	RTI effect	(dimensionless)
u_2	PI effect	(dimensionless)

2.5.3 HIV-1 Infection Model Analysis

For simplicity, T, T^* and ν shall be represented by X_1, X_2 and X_3, respectively, and all the parameters needed will be included in $\boldsymbol{\theta}$, so that one has:

$$\mathbf{X} \triangleq (X_1, X_2, X_3)' \tag{2.9}$$

$$\boldsymbol{\theta} \triangleq (s, d, \beta, \mu, k, c, u_1, u_2)' \tag{2.10}$$

$$\dot{\mathbf{X}} = \mathbf{f}(\mathbf{X}, \boldsymbol{\theta}) \tag{2.11}$$

Before the infection, $X_2 = X_3 = 0$, meaning that uninfected cells approach the equilibrium $X_1 = s/d$. At $t = 0$, when the infection occurs, the virus population count becomes ν_0. This means that the initial conditions for an infected patient are

$$\begin{array}{rcl} X_1(0) & = & s/d \\ X_2(0) & = & 0 \\ X_3(0) & = & \nu_0 \end{array} \tag{2.12}$$

It is also assumed that when the infection occurs, the patient has not been prescribed any antiretroviral drugs, and therefore $u_1 = u_2 = 0$.

For the infection to take, the crucial quantity to be measured is the basic reproductive ratio, R_0, which is defined as the number of newly infected cells that arise from any one infected cell, when almost all cells are uninfected [6], given by

$$R_0 = \frac{\beta k}{\mu c} X_1(0) = \frac{\beta k s}{\mu c d} \tag{2.13}$$

If $R_0 < 1$, the infection will not spread, since any infected cell will produce, on average, less than one other infected cell. On the other hand, if $R_0 > 1$, the infection will succeed, generating an exponencial multiplication of the virus [11].

Another factor that contributes to the model analysis is the existence (or not) of equilibrium points. The model presented in (2.8) has two equilibrium points that can be obtained computing $\mathbf{f}(\mathbf{X}, \boldsymbol{\theta}) = 0$. For a complete reasoning on the equilibrium points analytical expression, refer to Appendix B.

$$\begin{array}{rcl} \overline{\mathbf{X}}^1 & = & \left(\frac{s}{d}, 0, 0\right) \\ \overline{\mathbf{X}}^2 & = & \left(\frac{\mu c}{\beta k}, \frac{s}{\mu} - \frac{dc}{\beta k}, \frac{sk}{\mu c} - \frac{d}{\beta}\right) \end{array} \tag{2.14}$$

These equilibrium points (and especially the endemic one), do not depend on any initial conditions, but only on $\boldsymbol{\theta}$. Nevertheless, initial conditions are important because they give very relevant information on the current state of the patient, and how fast he will evolve to the equilibrium point.

The model also shows that the endemic equilibrium is a stable one, and that the healthy equilibrium is an unstable one [7, 12, 39]. This is, in fact, what happens in HIV-1 infection, where only a very small amount of virus is needed to initiate the infection.

Throughout this work, it is assumed that treatment always starts after the equilibrium point has been reached. Moreover, the model proposed in (2.8) does not account for the AIDS stage of the HIV-1 infection, in which there is a rapid decline in healthy CD4+ T cell count, while the virus load rises abruptly. The treatment that is currently available has the purpose of bringing the viral load to a very low value (50 copies mm^{-3}). This is, in fact, the measure for success or failure of a virological treatment for HIV-1 infection. This is based on the understanding that, the more rapid and greater the decrease in viral load, the longer the therapeutic effect holds [6].

To illustrate the model behavior, an example using a parameter set from [12] is simulated.

$$\boldsymbol{\theta} = \left(\ 9,\ 0.009,\ 4 \times 10^{-6},\ 0.3,\ 80,\ 0.6\ \right)' \tag{2.15}$$

The initial conditions used follow from (2.12).

$$\mathbf{X}_0 = \mathbf{X}(0) = \begin{bmatrix} 1000 \\ 0 \\ 1 \end{bmatrix} \tag{2.16}$$

This example assumes that no medication is used, and therefore $u_1 = u_2 = 0$ throughout the whole simulation. For this set of parameters, $R_0 = 1.78$, which means that the infection is supposed to succeed. The results are represented in Figure 2.8.

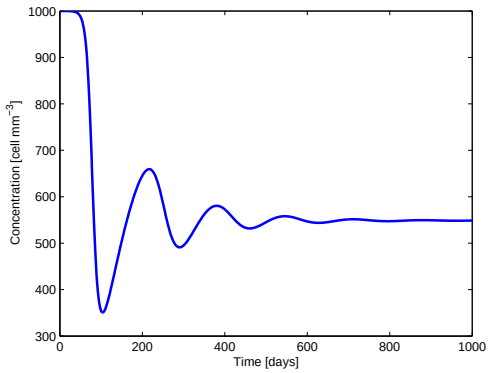

(a) Healthy CD4+ T cells

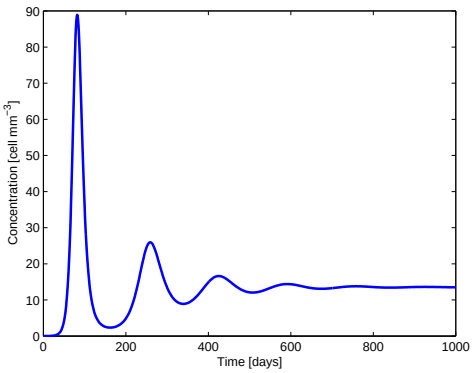

(b) Infected CD4+ T cells

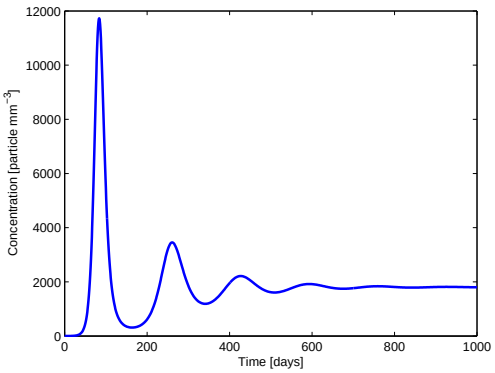

(c) Free Virus Particles

Figure 2.8: HIV-1 dynamic model simulation for parameter set in (2.15) and initial conditions in (2.16).

Results show that there is an exponential growth on virus load in the early stages of infections, accompanied by a quick drop on healthy CD4+ T cell count. After this first peak, the virus load and T cell count oscillate and eventually reach an equilibrium point, which may be predicted by (2.14).

$$\mathbf{X}_{eq} = \begin{bmatrix} 562.5 \\ 13.125 \\ 1750 \end{bmatrix} \tag{2.17}$$

2.5.4 Comparative Study between parameter sets

As it is seen above, one of the model properties that depends on the parameter set chosen is the equilibrium point. In fact, this property is determined exclusively by the model parameters.

In this Section, other sets are tested in order to assess what other features depend on the model parameters.

The first parameter set is from [38], and is given by

$$\boldsymbol{\theta}_1 = \begin{pmatrix} 10,\ 0.02,\ 2.4 \times 10^{-5},\ 0.24,\ 100,\ 2.4 \end{pmatrix}' \tag{2.18}$$

To make sure that the infection behavior depends as much as possible on the parameter set, the initial conditions used follow from (2.12), as did those in the previous simulation.

$$\mathbf{X}_0 = \mathbf{X}^{(1)}(0) = \begin{bmatrix} 500 \\ 0 \\ 1 \end{bmatrix} \tag{2.19}$$

In this case, $R_0 = 2.08$, meaning that the infection for this parameter set is supposed to be more aggressive than for the previous simulation. The results are represented in Figure 2.9.

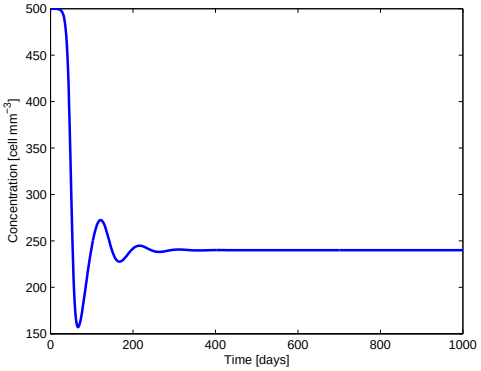

(a) Healthy CD4+ T cells

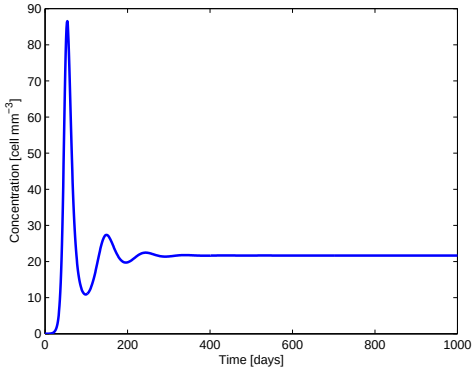

(b) Infected CD4+ T cells

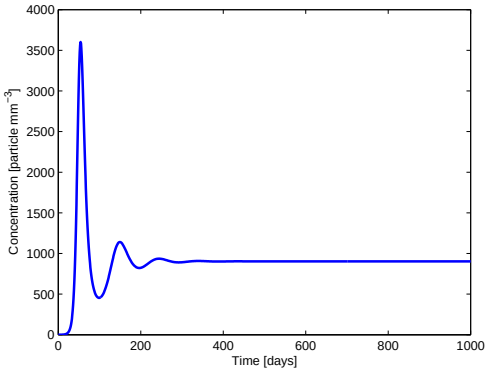

(c) Free Virus Particles

Figure 2.9: HIV-1 dynamic model simulation for parameter set in (2.18) and initial conditions in (2.19).

The next parameter set reflects the possibility of having a particularly infectious HIV-1 strain. This may be reflected in the increase of parameter β, resulting in

$$\boldsymbol{\theta}_2 = \begin{pmatrix} 9, & 0.009, & 4 \times 10^{-5}, & 0.3, & 80, & 0.6 \end{pmatrix}' \tag{2.20}$$

Since the initial conditions do not depend on β, the values in (2.16) hold for this simulation. For this parameter set, $R_0 = 17.8$. This high value indicates that the virus growth will occur in early stages of the infection. The results are shown in Figure 2.10.

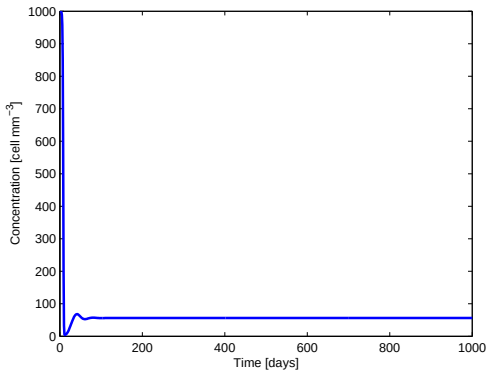

(a) Healthy CD4+ T cells

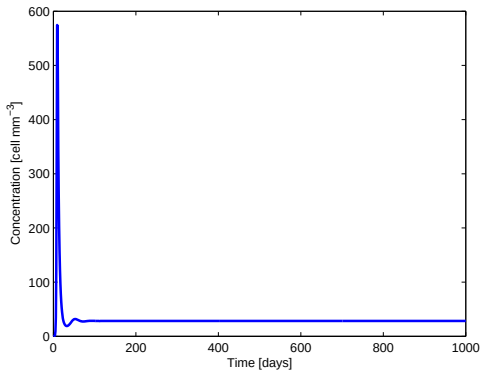

(b) Infected CD4+ T cells

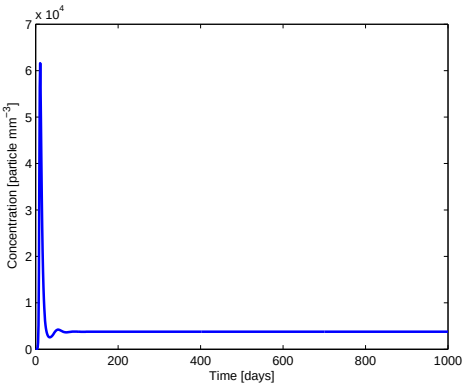

(c) Free Virus Particles

Figure 2.10: HIV-1 dynamic model simulation for parameter set in (2.20) and initial conditions in (2.16).

Finally, the last parameter set reflects the possibility of having a particularly resistant HIV-1 strain. This may be reflected in the increase of parameter c, resulting in

$$\boldsymbol{\theta}_3 = \begin{pmatrix} 9, & 0.009, & 4 \times 10^{-6}, & 0.3, & 80, & 0.2 \end{pmatrix}' \tag{2.21}$$

Since the initial conditions do not depend on c, the values in (2.16) hold for this simulation. For this parameter set, $R_0 = 5.3$. This value is high when compared to the first simulation, but not as high as the previous one. Results are shown in Figure 2.11.

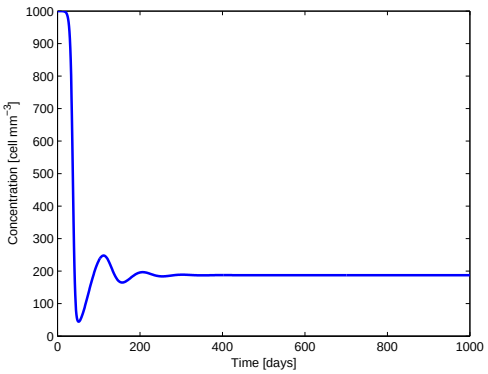

(a) Healthy CD4+ T cells

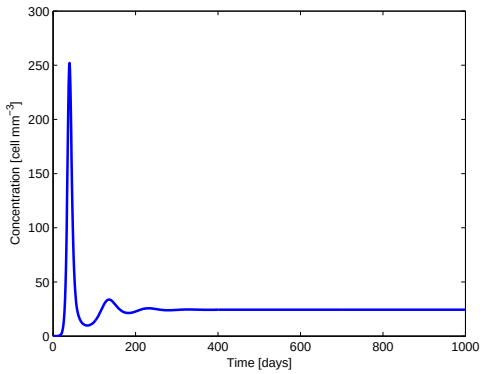

(b) Infected CD4+ T cells

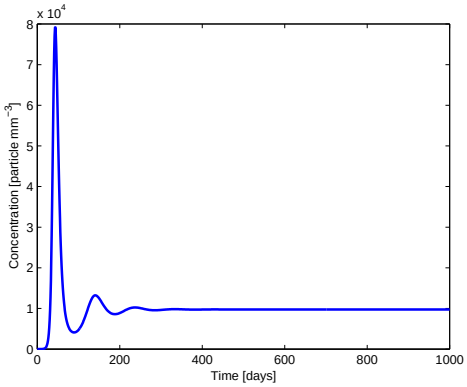

(c) Free Virus Particles

Figure 2.11: HIV-1 dynamic model simulation for parameter set in (2.21) and initial conditions in (2.16).

Comparing the results from Figures 2.8 through 2.11, it is possible to see that the most aggressive infections result from the parameter sets in (2.20) and (2.21). When the value of β is increased, the time period before the first viral peak is greatly shortened. However, it is when c is lowered that the virus load reaches its highest peak.

Concerning the time before the first viral peak occurs, the simulations are ranked as follows: first, Figure 2.10, with the peak occurring after 11 days; then, Figure 2.11, with 44 days; after that, Figure 2.9, with a period of 54 days; and finally, Figure 2.8, with a 88 day period before the virus load peaks. This order is expectable, since it is closely related to R_0. The value for this property is ranked in the same order as the time until the first virus peak occurs. R_0 represents the number of newly infected cells that arise from any one infected cell, when almost all cells are uninfected, meaning that this property describes the virus load exponential growth in the beginning of the infection.

Another property mentioned above is the value of the first viral peak. According to this property, the simulation with the highest virus peak is the one in Figure 2.11. After that, the

simulation in Figure 2.10 has the second highest virus peak, followed by Figure 2.8 and Figure 2.9.

The last property studied for these simulations are the time required for the equilibrium to be reached. In this work, it is considered the time instant in which the magnitude of oscillations are less than 10% of the final equilibrium point. The parameter set that takes the longest to reach equilibrium is the first (535 days), followed by the last one (198 days). The second parameter set takes 168 days to reach equilibrium, and the third set, represented in Figure 2.10, takes only 58 days to reach a state of equilibrium.

2.5.5 Other HIV-1 Infection Models

2.5.5.A Model with Proliferative T cells and Latent Infection

The assumption that CD4+ T cells do not proliferate made in the previous Section is an approximation. This model overcomes this situation by adding the extra term to allow cell proliferation. Moreover, it considers the existence of two infected CD4+ T cell populations: latently infected CD4+ T cells (L) and actively infected CD4+ T cells (T^*). The proposed model, which is fully described in [7, 15], also considers healthy CD4+ T cells (T) and free virus particles (ν), as does the model in (2.8).

$$\begin{cases} \dot{T} &= s - dT + pT\left(1 - \frac{T_{\text{tot}}}{T_{\max}}\right) - (1-u_1)\beta T\nu \\ \dot{L} &= (1-u_1)\beta T\nu - dL - \beta_L L \\ \dot{T^*} &= \beta_L L - \mu T^* \\ \dot{\nu} &= (1-u_2)kT^* - (1-u_1)\beta' T\nu - c\nu \end{cases} \tag{2.22}$$

where T_{tot} represents the total count of CD4+ T cells ($T_{\text{tot}} = T + L + T^*$). The majority of the model parameters are already described in Table 2.1. The remaining parameters (p, $T_{\max}$, μ_L, β_L, β') are concerned with the extra state introduced (L) and the extra terms in the already existing states. Parameter p represents the average per capita proliferation rate of healthy CD4+ T cells, that shuts off when $T_{\text{tot}} = T_{\max}$. β_L represents the average per capita activation rate of latently infected CD4+ T cells into virus particles, and β' has the same numerical value as β, but with different units. These parameters are summarized in Table 2.2.

Table 2.2: Parameter description for the HIV-1 infection model in (2.22). To be noted that T, L and T^* are measured in cell mm^{-3} and ν is measured in particle mm^{-3}.

Parameter	Description	Reference Value [7]
p	average per capita growth rate of healthy CD4+ T cells	0.03 day^{-1}
$T_{\max}$	maximum CD4+ cell count	1500 cell mm^{-3}
β_L	average per capita activation rate of latently infected CD4+ T cells	0.08 day^{-1}
β'	infection rate coefficient (same as β)	4×10^{-6} cell^{-1} mm^3 day^{-1}

2.5.5.B Model with Macrophages

CD4+ T cells are, by far, the most targeted cells by HIV-1 infection. However, experimental data in [15] suggests that there is more than one source of virus particles during the infection. Other cells, apart from CD4+ T cells, are known to be susceptible to HIV-1. One such pool of cells are macrophages. Some of these cells are CD4+, and may become actively infected by HIV-1. Moreover, HIV-1 infection tends not to kill macrophages, and they are able to produce virus particles longer than CD4+ T cells.

This model, proposed by Nelson and Perelson [15], is composed of 5 states: healthy CD4+ T cells (T), infected CD4+ T cells (T^*), healthy macrophages (M), infected CD4+ macrophages (M^*) and free virus particles (ν).

$$\begin{cases} \dot{T} &= s - dT - (1-u_1)\beta T\nu \\ \dot{T}^* &= (1-u_1)\beta T\nu - \mu T^* \\ \dot{M} &= s_M - d_M M - (1-u_1)\beta_M M\nu \\ \dot{M}^* &= (1-u_1)\beta_M M\nu - \mu_M M^* \\ \dot{\nu} &= (1-u_2)(kT^* + k_M M^*) - c\nu \end{cases} \tag{2.23}$$

where $T_{\text{tot}} = T + T^*$. Most of the model parameters are already described in Table 2.1 and 2.2. The rest of the parameters (s_M, d_M, β_M, μ_M, k_M) are concerned with the two extra states introduced, M and M^*. s_M represents the rate at which macrophages are created, while d_M represents their average *per capita* death rate. β_M is the rate at which macrophages become infected, while μ_M expresses the average per capita death rate of infected macrophages. Finally, k_M represents the rate at which macrophages produce new virus particles. These parameters are summarized in Table 2.3.

Table 2.3: Parameter description for the HIV-1 infection model in (2.23). To be noted that T, M, T^* and M^* are measured in cell mm^{-3} and ν is measured in particle mm^{-3}.

Parameter	Description	Reference Values [40]
s_M	healthy CD4+ macrophages replenishment rate	3 cell mm^{-3} day^{-1}
d_M	average per capita death rate of healthy CD4+ macrophages	0.1 day^{-1}
β_M	macrophages infection rate coefficient	8×10^{-7} particle^{-1} mm^3 day^{-1}
μ_M	average per capita death rate of infected CD4+ macrophages	0.02 day^{-1}
k_M	virus production rate coefficient	20 particle cell^{-1} day^{-1}

2.5.6 Comparative Study Between HIV-1 Infection Models

One way to compare dynamic models is to look at its space state trajectories, that refers to the space where the axis are the state variables. In this case, and to allow for a comparison with the model in (2.8), it is necessary to plot T, T^* and ν (or its equivalents) for each model. On the

other hand, it is also possible to compute the models equilibrium points, as a way of comparing their behavior. This steady state may indicate which model mimics the HIV-1 infection better.

2.5.6.A Model Space State Trajectories

For the model studied in this work, the space state trajectories are presented in Figure 2.12. In this plot, each line corresponds to a different set of initial conditions, and the model parameters are as in (2.15).

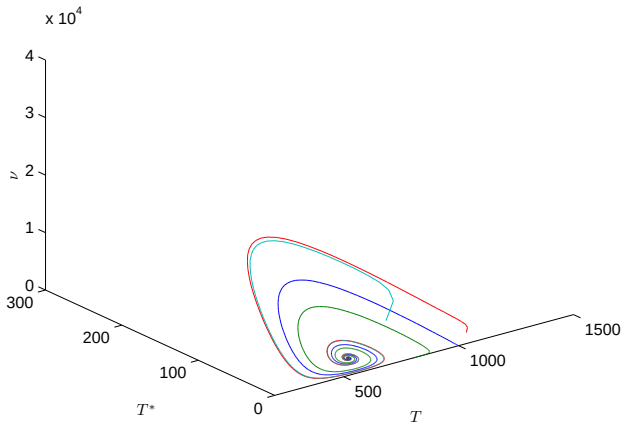

Figure 2.12: Space state trajectories for the model in (2.8) considering T, T^* and ν. The blue trajectory represents the set of initial conditions in (2.12).

From these trajectories, one conclusion is straightforward: the equilibrium point does not depend on the initial conditions, but only on the parameter set, as it was stated in (2.14). Moreover, for all trajectories, the model behavior is similar, with alternating peaks of healthy CD4+ T cells and virus particles, until an equilibrium is reached.

For the second model considered, it is necessary to take into account that the infected pool of cells is now divided in two: latently and actively infected CD4+ T cells. Therefore it is necessary to use $L + T^*$ instead of just T^* for the space trajectories. The results are presented in Figure 2.13. Again, each line corresponds to a different set of initial conditions. The parameter set is a combination of those in (2.15) and the ones presented in Table 2.2.

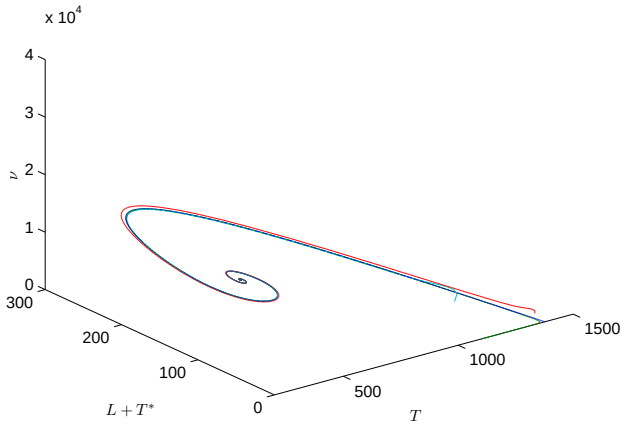

Figure 2.13: Space state trajectories for the model in (2.22) considering T, $L + T^*$ and ν.

Once again, there is only one equilibrium point, that does not depend on the initial conditions. The model behavior is similar to Figure 2.12, with oscillation for every model state. However, since this model considers two populations infected cells, the count of $L + T^*$ is higher than the count of T^* of the previous model. Moreover, because T cell proliferation is modeled, healthy CD4+ T cell count is also higher. Finally, the viral load peak is lower, but the steady state is larger than that of the previous model.

The third model considers not only CD4+ T cells but also a macrophage population. This means that there is an extra source of production of virus particles. The results are presented in Figure 2.14. Again, each line corresponds to a different set of initial conditions. The parameter set is a combination of those in (2.15) and the ones presented in Table 2.3.

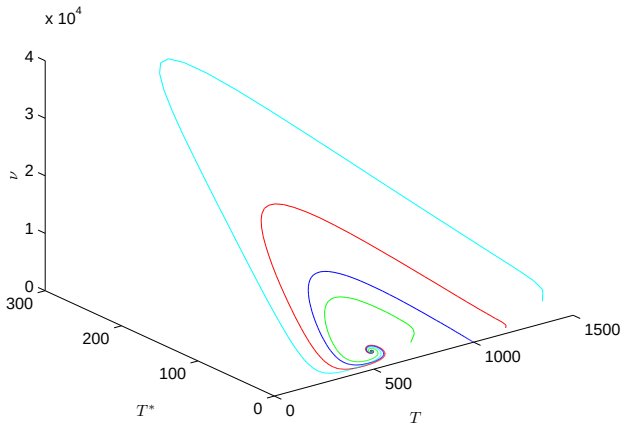

Figure 2.14: Space state trajectories for the model in (2.23) considering T, T^* and ν.

Analyzing these results, it can be seen that this model also exhibits a single equilibrium point,

as did the other models, and also has an oscillatory behavior around that equilibrium point. However, when compared to the previous model, the main difference lies in the viral load, that becomes significantly higher in this last model. This happens because of the extra source of virus particles (the macrophages) that add to those already produced by T cells. As a result, this model may be better to account for higher viral loads, without affecting T cell dynamics to a large extent, since the extra production comes from a different population.

2.5.6.B Model Equilibrium Points

For all the models considered above, it is possible to compute their equilibrium points analytically (by computing $\mathbf{f}(\mathbf{X}, \boldsymbol{\theta}) = 0$, which is done in Appendix B) or numerically. For the first model, this is already computed in (2.17). For the second model, that considers T cell proliferation and latently infected CD4+ T cells, the steady state is given by

$$\mathbf{X}_{eq}^{(1)} = \begin{bmatrix} 628.3 \\ 136.3 \\ 36.4 \\ 4827 \end{bmatrix} \tag{2.24}$$

For the last model, that considers the macrophage population, the steady state is given by

$$\mathbf{X}_{eq}^{(2)} = \begin{bmatrix} 540.4 \\ 13.8 \\ 29.5 \\ 2.3 \\ 1914.5 \end{bmatrix} \tag{2.25}$$

Analyzing the equilibrium points obtained for each model, it is possible to conclude that the models do not differ very much from each other, since all values are in the same order of magnitude. For the healthy CD4+ T cell population, all models predict that the equilibrium point is in the range of 500-700 cell mm^{-3}. This value is reasonable from experimental data, even though variance across patients is very large, and even for the same patient T cell counts can vary 5-15% daily. The fact that CD4+ T cell count can vary, even for the same patient, is a feature that none of these models considers. Therefore, the equilibrium points reached are satisfactory and mimic the reality well. As for the virus load, the equilibrium points are slightly more different, even though they are all in the same order of magnitude. However, the last two models allow to account for higher experimental virus loads, while the first model predicts a lower value. This is reflected by the fact that there are more infected populations considered in the last two models. In one of them, latently infected cells (that have the same life span as unifected cells) are modeled, increasing the number of cells that can become active and produce virus particles. In the other, another source of virus particles is introduced, which naturally leads to the increase in virus load. As the complexity of the models increases, it is likely that they mimic the infection dynamics better. However, the simplest model represents the HIV-1 infection satisfactorily, and its properties are simpler to study and better documented. That is why this model was chosen for further analysis in this work.

3

Model Sensitivity and Local Identifiability Analysis

Contents

Sensitivity and Identifiability analysis are valuable tools in experimental therapy design. Sensitivity provides information about the best time periods to make measurements, while identifiability is useful to assess which parameters from the model are possible to be estimated from experimental data. In this chapter, both analysis are performed for a particular case of study for the HIV-1 infection.

3.1 Model Sensitivity Analysis

Sensitivity analysis is the study of how input variation affects the output. For the model defined in (2.11), the objective is to study how variations in $\boldsymbol{\theta} = (s\ d\ \beta\ \mu\ k\ c)'$ affect the outcome $\mathbf{X} = (X_1, X_2, X_3)'$. Sensitivity computation is one of the tools that may help design clinical experiences, in order to achieve better outcomes [12]. By definition [12], the sensitivity of $\mathbf{X}$ with respect to an arbitrary parameter p is defined as

$$\mathbf{S}_p = \left.\frac{\partial \mathbf{X}}{\partial p}\right|_{p=p_0} \tag{3.1}$$

where p_0 is the nominal value for p, at which the sensitivity is computed. However, in this work, the interest lies in the sensitivity with respect to all parameters at once, and not only one. Therefore, the goal is to compute $\frac{\partial \mathbf{X}}{\partial \boldsymbol{\theta}}$ for $\boldsymbol{\theta} = \boldsymbol{\theta}_0$. If one derives (2.11) in order to $\boldsymbol{\theta}$, the result yields

$$\left.\frac{\partial \dot{\mathbf{X}}}{\partial \boldsymbol{\theta}}\right|_{\boldsymbol{\theta}=\boldsymbol{\theta}_0} = \left.\frac{\partial}{\partial \boldsymbol{\theta}}\mathbf{f}\left(\mathbf{X}, \boldsymbol{\theta}\right)\right|_{\boldsymbol{\theta}=\boldsymbol{\theta}_0} = \left.\left(\frac{\partial \mathbf{f}}{\partial \mathbf{X}}\frac{\partial \mathbf{X}}{\partial \boldsymbol{\theta}}\right)\right|_{\boldsymbol{\theta}=\boldsymbol{\theta}_0} + \left.\frac{\partial \mathbf{f}}{\partial \boldsymbol{\theta}}\right|_{\boldsymbol{\theta}=\boldsymbol{\theta}_0} \tag{3.2}$$

Now, if $\boldsymbol{\theta}$ does not change over time, it is true that [12, 41]

$$\frac{\partial}{\partial \boldsymbol{\theta}}\dot{\mathbf{X}} = \frac{d}{dt}\frac{\partial \mathbf{X}}{\partial \boldsymbol{\theta}} \tag{3.3}$$

which leads to a differential equation for $\frac{\partial \mathbf{X}}{\partial \boldsymbol{\theta}}$. Defining

$$\mathbf{S} = \left.\frac{\partial \mathbf{X}}{\partial \boldsymbol{\theta}}\right|_{\boldsymbol{\theta}=\boldsymbol{\theta}_0} \tag{3.4}$$

it follows that

$$\dot{\mathbf{S}} = \left.\frac{\partial \mathbf{f}}{\partial \mathbf{X}}\right|_{\boldsymbol{\theta}=\boldsymbol{\theta}_0} \cdot \mathbf{S} + \left.\frac{\partial \mathbf{f}}{\partial \boldsymbol{\theta}}\right|_{\boldsymbol{\theta}=\boldsymbol{\theta}_0} \tag{3.5}$$

Expressions for $\frac{\partial \mathbf{f}}{\partial \mathbf{X}}$ and $\frac{\partial \mathbf{f}}{\partial \boldsymbol{\theta}}$ can be derived analytically. These are given by

$$\frac{\partial \mathbf{f}}{\partial \mathbf{X}} = \begin{bmatrix} -d - \beta\nu & 0 & -\beta T \\ \beta\nu & -\mu & \beta T \\ 0 & k & -c \end{bmatrix} \tag{3.6}$$

$$\frac{\partial \mathbf{f}}{\partial \boldsymbol{\theta}} = \begin{bmatrix} 1 & -T & -T\nu & 0 & 0 & 0 \\ 0 & 0 & T\nu & -T^* & 0 & 0 \\ 0 & 0 & 0 & 0 & T^* & -\nu \end{bmatrix} \tag{3.7}$$

As done in [12], (3.5) can be solved numerically, assuming that $\mathbf{S}(0) = \mathbf{0}$. However, this may not be the correct initial value for $\mathbf{S}(0)$. Recalling (2.12), initial conditions depend on $\boldsymbol{\theta}$, and therefore $\mathbf{S}(0)$ is not necessarily $\mathbf{0}$. Using (3.4), one finds that

$$\begin{aligned} \mathbf{S}(0) &= \frac{\partial \mathbf{X}(0)}{\partial \boldsymbol{\theta}} \\ \mathbf{S}(0) &= \begin{bmatrix} 1/d & -s/d^2 & 0 & 0 & 0 & 0 \\ 0 & 0 & 0 & 0 & 0 & 0 \\ 0 & 0 & 0 & 0 & 0 & 0 \end{bmatrix} \end{aligned} \tag{3.8}$$

The variable $\mathbf{S}$ should not be confused with $\mathbf{S}_p$. While the sensitivity with respect to a particular parameter has $N \times n$ entries, $\mathbf{S}$ has $N \times n \times q$ components (N being the number of states of the model, n the number of simulation time points, and q the number of parameters). This means that $\mathbf{S}_p$ is a second-order tensor (matrix), while $\mathbf{S}$ is a third-order tensor [12]. However, in this work, $\mathbf{S}$ is rearranged as a matrix, since this is required for a later identifiability analysis (in Section 3.2). Hence, as done in [42],it is defined that

$$\mathbf{S}^m(Nn, q) = \mathbf{S}(N, n, q) \tag{3.9}$$

3.1.1 Sensitivity Numerical Simulations

The sensitivity simulations are performed using the parameter set in (2.15) and the initial conditions in (2.16) and (3.9), by solving (2.11) and (3.5) simultaneously. The results obtained are represented in Figure 3.1.

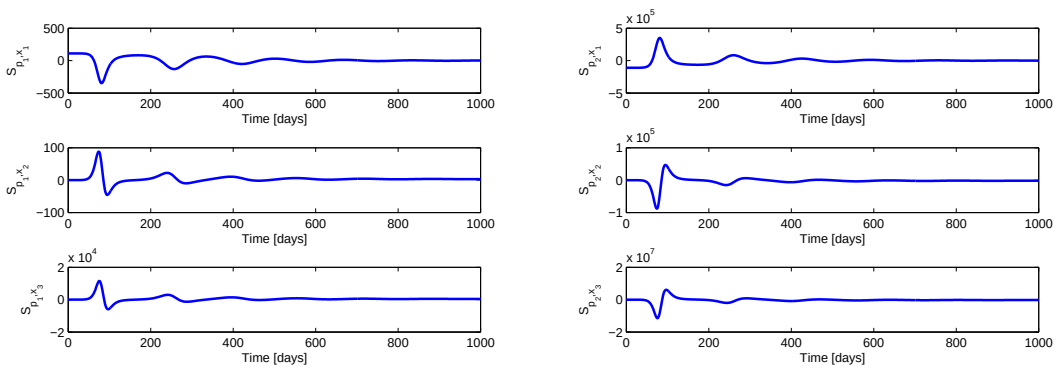

(a) s **(b)** d

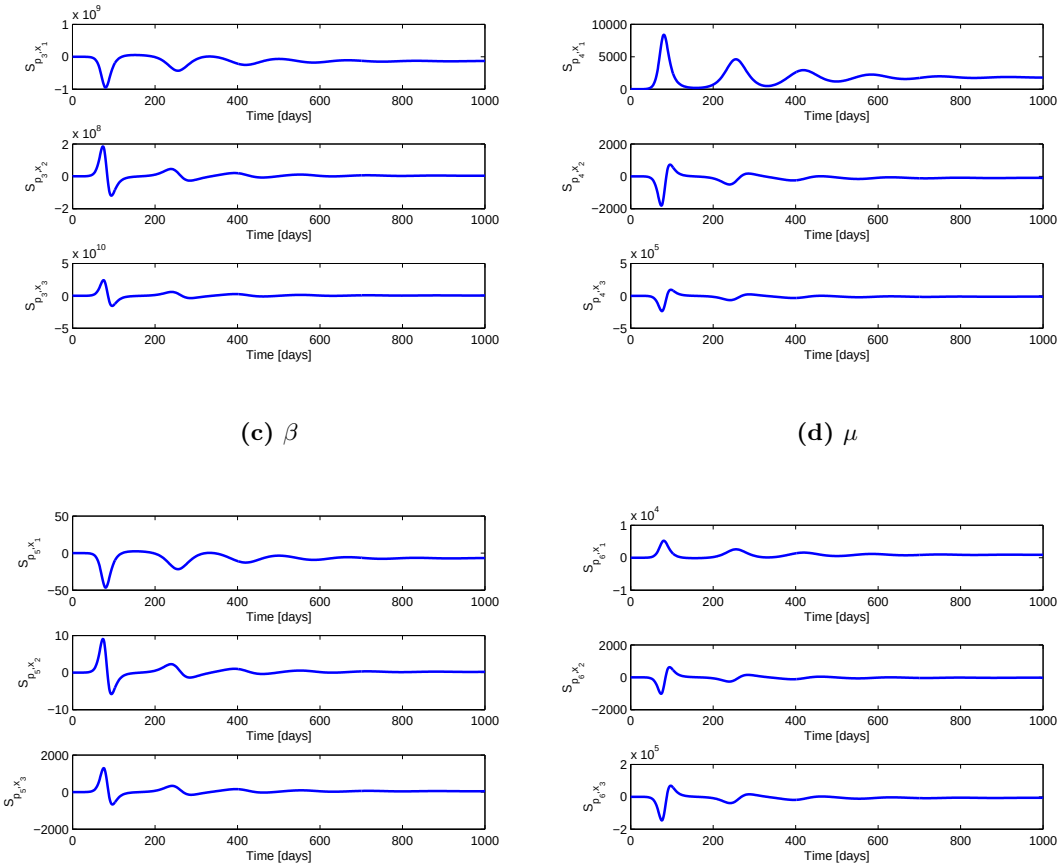

(c) β **(d)** μ

(e) k **(f)** c

Figure 3.1: Time evolution of the sensitivities for all states, for each parameter.

Analyzing these results, it can be seen that the most informative time period is between the 50^{th} and 100^{th} day, since it is in this interval that the sensitivities have higher absolute values (it should be remarked that this depends on the value of model parameters and on the initial state conditions). After this, there are some periods where measurements carry relevant information, whereas there are others where the sensitivity is close to zero. Finally, measurements made after 600 days carry little or no information about the parameters, since the sensitivity values are practically zero for all parameters.

Sensitivity results are useful in therapy design since they provide with valuable data that supports the decision of when measurements should be made (in the HIV-1 case, when blood samples should be drawn). If measurements are made on the right timing, the output will be most sensitive to the parameters, and the reverse engineering step of estimating the parameters will be easier.

3.2 Local Identifiability Analysis

The fact that good experimental data is available does not guarantee that the estimation is possible. Even though necessary, a good data set is not sufficient to ensure estimability. It is also necessary to perform a local identifiability analysis that will tell if the model is identifiable from experimental data or not.

Identifiability is a basic system property that determines whether all parameters can be uniquely estimated based on measured outputs [23]. However, even if a system is not identifiable, there may still be a subset of identifiable parameters.

A dynamic system is identifiable if $\boldsymbol{\theta}$ can be uniquely determined from the measurable system output $\mathbf{X}$; otherwise, it is said to be unidentifiable [24]. However, identifiability may be global or local. A system is said to be globally identifiable if for any two parameter vectors $\boldsymbol{\theta}_1$ and $\boldsymbol{\theta}_2$, $\mathbf{X}_1 = \mathbf{X}_2$ holds if and only if $\boldsymbol{\theta}_1 = \boldsymbol{\theta}_2$. On the other hand, a system is said to be locally identifiable if for any two parameter vectors $\boldsymbol{\theta}_1$ and $\boldsymbol{\theta}_2$ in the neighborhood of some point $\boldsymbol{\theta}^*$, $\mathbf{X}_1 = \mathbf{X}_2$ holds if and only if $\boldsymbol{\theta}_1 = \boldsymbol{\theta}_2$ [24, 43]. In this work, the concern is about the study of local identifiability.

Local identifiability can be studied in several ways. In this work, two different methods are used: the analysis of the sensitivity correlation matrix, and the sensitivity matrix Singular Value Decomposition (SVD).

3.2.1 Correlation Matrix Analysis

A classic way of studying parameter identifiability is through the sensitivity correlation matrix $\mathbf{R}$, that represents a measure of linear inter-dependence for the columns of the sensitivity time-evolution [44, 45]. The Pearson's correlation coefficient between two variables P and Q is defined as the covariance of the two variables divided by the product of their standard deviations.

$$\rho(P,Q) = \operatorname{corr}(P,Q) = \frac{\operatorname{cov}(P,Q)}{\sigma_P \sigma_Q} = \frac{E[(P-\mu_P)(Q-\mu_Q)]}{\sigma_P \sigma_Q} \tag{3.10}$$

where μ and σ denote for the mean and the standard deviation, respectively. For finite samples this can be approximated with the sample correlation coefficients

$$r(P,Q) = \frac{\sum_{i=1}^{n}(P_i - \bar{P})(Q_i - \bar{Q})}{\sqrt{\sum_{i=1}^{n}(P_i - \bar{P})^2}\sqrt{\sum_{i=1}^{n}(Q_i - \bar{Q})^2}} \tag{3.11}$$

The correlation matrix is given by

$$R_{ij} = r(\mathbf{S}^m_{.i}, \mathbf{S}^m_{.j}) \tag{3.12}$$

where the notation $\mathbf{S}^m_{.i}$ represents the i-th column of $\mathbf{S}^m$.

As the correlation matrix is symmetric ($\rho(P,Q) = \rho(Q,P)$), $\mathbf{R}$ is symmetric. Moreover, since $\rho(P,P) = 1$, diagonal elements in $\mathbf{R}$ are all 1. As to the rest of the elements (the non-diagonal

ones), they indicate whether the model is or is not identifiable. If these elements are close to 0, it indicates good identifiability, since the sensitivity matrix columns are independent of each other, and input variations in one parameter will be uniquely reflected in the output. On the other hand, if these coefficients are close to either 1 or -1 (which is the maximum value they can take), it means that the columns of $\mathbf{S}^m$ have strong linear correlation or anti-correlation, respectively. Therefore, the model is not identifiable [44].

In order to analyze how this method can be applied to the model in study, a simulation is performed. The HIV-1 infection model to be solved is given by

$$\begin{cases} \dot{T} &= s - dT - \beta T\nu \\ \dot{T}^* &= \beta T\nu - \mu T^* \\ \dot{\nu} &= kT^* - c\nu \end{cases} \tag{3.13}$$

Simultaneously, it is necessary to couple to this model the sensitivity equations in (3.5),

$$\dot{\mathbf{S}} = \left.\frac{\partial \mathbf{f}}{\partial \mathbf{X}}\right|_{\boldsymbol{\theta}=\boldsymbol{\theta}_0} \cdot \mathbf{S} + \left.\frac{\partial \mathbf{f}}{\partial \boldsymbol{\theta}}\right|_{\boldsymbol{\theta}=\boldsymbol{\theta}_0} \tag{3.14}$$

where the parameter set is given by $\boldsymbol{\theta} = \left(9,\ 0.009,\ 4\times10^{-6},\ 0.3,\ 80,\ 0.6\right)'$. As for the initial conditions, these are given by (2.16) and (3.9),

$$\begin{array}{rcl} X_1(0) &=& s/d \\ X_2(0) &=& 0 \\ X_3(0) &=& \nu_0 \end{array} \tag{3.15}$$

$$\begin{aligned} \mathbf{S}(0) &= \frac{\partial \mathbf{X}(0)}{\partial \boldsymbol{\theta}} \\ &= \begin{bmatrix} 1/d & -s/d^2 & 0 & 0 & 0 & 0 \\ 0 & 0 & 0 & 0 & 0 & 0 \\ 0 & 0 & 0 & 0 & 0 & 0 \end{bmatrix} \end{aligned} \tag{3.16}$$

The sampling frequency for the simulation was 1 point per day, starting at $t = 0$ and ending at $t = 1000$. The correlation of $\mathbf{S}^m$ is computed using (3.12), and the results obtained are given by

$$\mathbf{R} = \begin{bmatrix} 1 & -0.98745 & 0.98991 & -0.98514 & 0.9995 & -0.99681 \\ -0.98745 & 1 & -0.98396 & 0.958 & -0.98564 & 0.97801 \\ 0.98991 & -0.98396 & 1 & -0.95447 & 0.98885 & -0.9782 \\ -0.98514 & 0.958 & -0.95447 & 1 & -0.98777 & 0.99541 \\ 0.9995 & -0.98564 & 0.98885 & -0.98777 & 1 & -0.99814 \\ -0.99681 & 0.97801 & -0.9782 & 0.99541 & -0.99814 & 1 \end{bmatrix} \tag{3.17}$$

From the results in (3.17), it is possible to see that the model is not identifiable, since all non-diagonal elements are very close to either 1 or -1. However, it is not possible to know whether there is an identifiable subset of parameters or not, or even which parameter is the hardest to identify. Given the fact that each R_{ij} represents the correlation of the i-th with the j-th columns of $\mathbf{S}^m$, the only conclusion that can be draw is that the model, in general, is not identifiable. In order to say which parameters it is possible to identify and which it is not, another approach to the study of local identifiability in an HIV-1 infection model is proposed in the next Section.

3.2.2 Singular Value Decomposition

Any arbitrary real $m \times n$ matrix $\mathbf{M}$ can be decomposed into the product of three other matrices

$$\mathbf{M} = \mathbf{U}\Sigma\mathbf{V}^{\mathrm{T}} \tag{3.18}$$

where $^{\mathrm{T}}$ denotes the transpose matrix, and $\mathbf{U}$ and $\mathbf{V}$ are real square unitary matrices [1], with dimensions $m \times m$ and $n \times n$, respectively, and Σ is an $m \times n$ nonnegative real diagonal matrix. Such a factorization is called the Singular Value Decomposition (SVD) of $\mathbf{M}$. $\mathbf{U}$ and $\mathbf{V}$ are called the matrices of left and right singular vectors of $\mathbf{M}$, respectively, whereas the diagonal entries Σ_{ii} are the singular values of $\mathbf{M}$. By convention, the diagonal elements of Σ are constructed to be ordered in decreasing magnitude [46].

SVD can be examined from three points of view. First, it is a way of transforming correlated variables into a set of uncorrelated ones that better expose the various relationships in the original data. However, at the same time, it is a method for identifying and ordering dimensions along which data points exhibit most variation. Finally, it is also useful in data reduction, since when it is known the dimensions along which the variation is greatest, it is possible to find the best approximation of the original data using fewer dimensions. In this work, the two first points of view are of interest, while the latter one is not used.

SVD is also closely related to the standard eigenvalue-eigenvector decomposition of a square symmetric matrix. In fact, $\mathbf{U}$ is the matrix of eigenvectors of $\mathbf{M}\mathbf{M}^{\mathrm{T}}$, V is the matrix of eigenvectors of $\mathbf{M}^{\mathrm{T}}\mathbf{M}$, and the nonnegative elements of Σ are equal to the square root of the eigenvalues of $\mathbf{M}^{\mathrm{T}}\mathbf{M}$ [46].

For the case in study, the sensitivity matrix $\mathbf{S}^m$ allows the expression $\delta\mathbf{X} = \mathbf{S}^m\delta\boldsymbol{\theta}$ to hold. This means that absolute parameter variations are locally identifiable from experimental data if $\mathbf{S}^m$ has full rank [42]. Using SVD, the factorization $\mathbf{S}^m = \mathbf{U}^m\Sigma^m\mathbf{V}^{m\mathrm{T}}$ can be obtained. Taking in consideration that $\mathbf{U}^m$ and $\mathbf{V}^m$ are unitary matrices, $\mathbf{S}^m$ has full rank if all singular values of Σ^m are greater than zero. However, in numerical simulations (as it is the case), it is common that even though there are not any zero singular values, the smallest ones are, when compared to the largest, negligible. In other words, $\mathbf{S}^m$ may have full rank but still be ill-conditioned. In [43], a method is proposed to determine which parameters are identifiable and which are not. The rank of $\mathbf{S}^m$ is in practice determined by normalizing all singular values with respect to the largest, and then setting a cutoff, below which singular values are considered to be 0. Then, the (practically) unidentifiable parameter subspace is spanned by the last columns of $\mathbf{V}^m$ with "nearly" zero singular values [42].

This analysis represents an improvement when compared to the method referred earlier (Section 3.2.1), since it not only allows to determine whether the model is or is not identifiable, but it also can tell which parameter are the least identifiable.

[1] A real matrix $\mathbf{X}$ is unitary if and only if $\mathbf{X}^{\mathrm{T}}\mathbf{X} = \mathbf{I}$, or in other words, $\mathbf{X}^{\mathrm{T}} = \mathbf{X}^{-1}$.

In Figure 3.2 are represented the singular values of $\mathbf{S}^m$, for the model presented in (2.11) and (3.5), with the parameter set in (2.15), and initial conditions in (2.16) and (3.9). In this simulation, the cutoff used was 10^{-6}.

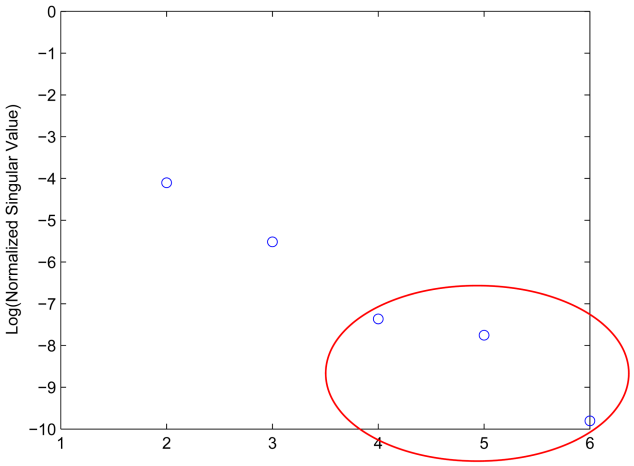

Figure 3.2: Normalized singular values for the sensitivity matrix $\mathbf{S}^m$, in a logarithmic scale. In red, the singular values below the cutoff value.

The results obtained show that there are, in fact, unidentifiable parameters (for the cutoff value chosen). To assess which are these parameters, it is necessary to inspect the last columns of $\mathbf{V}^m$.

$$\mathbf{V}^m = \begin{bmatrix} 0.0000 & -0.0005 & -0.0205 & 0.1565 & \mathbf{0.9875} & -0.0056 \\ 0.0004 & 0.9999 & -0.0172 & 0.0011 & 0.0000 & 0.0000 \\ -1.0000 & 0.0004 & 0.0000 & 0.0000 & 0.0000 & 0.0000 \\ 0.0000 & 0.0155 & 0.9219 & 0.3848 & -0.0419 & -0.0011 \\ 0.0000 & -0.0001 & -0.0024 & 0.0090 & 0.0042 & \mathbf{0.9999} \\ 0.0001 & 0.0076 & 0.3864 & \mathbf{-0.9096} & 0.1522 & 0.0085 \end{bmatrix} \tag{3.19}$$

The matrix $\mathbf{V}^m$ in (3.19) shows that the least unidentifiable parameter is the 5^{th}, k, followed be the 1^{st}, s, and the last one, c. This happens because the highest values in the last three columns (that correspond to the three singular values below the cutoff value considered) are for these three parameters. μ might also be considered as unidentifiable, given its relatively high value in the 4^{th} column (0.3848). However, since this is not clear, as the other three are, it was not considered to be unidentifiable.

The SVD appears to be a better method for local identifiability analysis than the correlation matrix. Even though the correlation method succeeds in saying that the model is not identifiable, it is not able to tell which parameters are the least identifiable. SVD, on the other hand, not only identifies the model as not being identifiable (since there are singular values below the cutoff, rendering $\mathbf{S}^m$ ill-conditioned), but also states which subset of parameters is not identifiable (in this case, for this parameter set and initial conditions, k, s and c). Once the not identifiable parameters are computed, it is possible to iteratively try to find a subset of identifiable parameters. One approach might be to set the least identifiable parameter with a reference value, and re-run the

algorithm, and see if there are still singular values below the cutoff value. If so, then the second least identifiable parameter would also be set to a reference value. The situation would continue until a subset of identifiable parameters was found, or when there was only one parameter left. In this situation, it would not be possible to identify any model parameters from experimental data. In this case, a model reparameterization may help in building an identifiable (or partially) identifiable model, with at least a subset of identifiable parameters [47].

4

Drug Kinetic and Dynamic Models

Contents

An important step in the construction of the HIV-1 infection dynamic model is the drug kinetic and dynamic behavior. In this Chapter, the fitting for the pharmacokinetic model described in Chapter 2 is performed, and the pharmacodynamic data for each drug presented. Afterwards, several simulations of the full model are performed, allowing for a comparison between different experimental conditions, namely, patient adherence, drug dosage, and drug administration frequency.

4.1 Antiretroviral Drug Model

In this work, two different drugs are considered: a RTI, lamivudine (3TC) and a PI, indinavir (IDV). For each chosen drug, it is necessary to find the respective pharmacokinetic and pharmacodynamic model (see Section 2.3.1 for further detail on these models). The reason why these two drugs were chosen was that they were the only two for which both kinetic and dynamic data could be found. 3TC is taken as a daily 300 mg pill (or in some cases a 150 mg twice a day), and is very commonly used for HIV-1 infection treatment [48]. On the other hand, IDV is taken as a 800 mg pill three times a day [48]. This is one of the reasons why IDV is becoming less and less used. It has a very strict schedule that the patient needs to follow, and the drug doses involved are very high, which may lead to intolerance or toxicity.

4.1.1 Drugs Pharmacokinetic Data and Model Fitting

Experimental pharmacokinetic data for 3TC is represented in Figure 4.1. In this experiment, a single dose of 300 mg is administered to patients at $t = 0$, and plasma concentration is then measured over the following 12 hours.

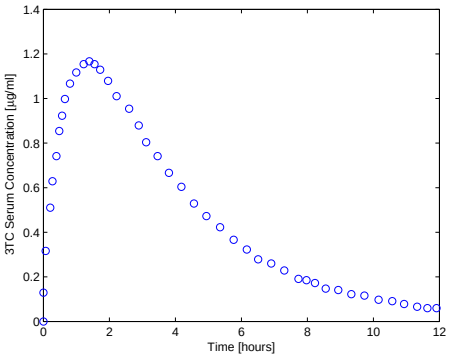

Figure 4.1: Lamivudine (3TC) serum concentrations over time, for an initial dose of 300 mg. Data adapted from [49].

As it is possible to see, the serum concentration of 3TC peaks between hours 1 and 2, after which it steadily drops, until only a residual quantity is present after 12 hours.

Regarding IDV, experimental pharmacokinetic data is represented in Figure 4.2. In this case, a dose of 800 mg is administered at the beginning of the experiment, and plasma concentration is then measured over 8 hours.

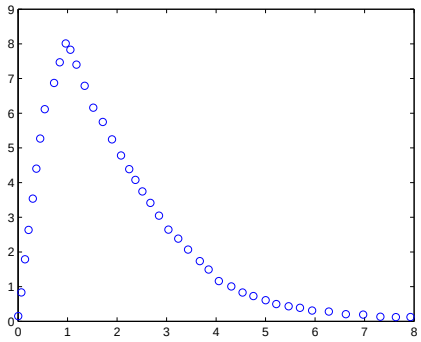

Figure 4.2: Indinavir (IDV) serum concentrations over time, for an initial dose of 800 mg. Data adapted from [50].

The kinetic behavior for IDV is very similar to that of 3TC presented in Figure 4.1. The main differences are that the plasma concentration peak is much sharper in this case (which may lead to difficulties in the model fitting) and the residual amount of drug after 8 hours is much lower (approximately zero) for IDV.

In order to incorporate pharmacokinetic data into the infection model, it is necessary to fit this data to the pharmacokinetic model in (2.1). For that, a particle swarm optimization algorithm is used [51][1], and the optimized parameters are, for 3TC and IDV, respectively,

$$\mathbf{A}_{3\text{TC}} = \begin{bmatrix} -0.3014 & 0.7817 \\ 9.35 \times 10^{-6} & -1.6391 \end{bmatrix} \tag{4.1}$$

$$\mathbf{A}_{\text{IDV}} = \begin{bmatrix} -1.0061 & 0.3702 \\ 2.41 \times 10^{-5} & -1.0060 \end{bmatrix} \tag{4.2}$$

The resulting fit created used with the kinetic parameters in (4.1) and (4.2) are represented in Figures 4.3 and 4.4.

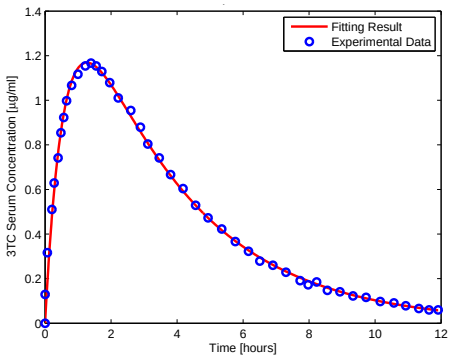

Figure 4.3: Lamivudine (3TC) experimental pharmacokinetic data fit, for an initial dose of 300 mg.

[1]The algorithm was used as a part of a MATLAB®toolbox, available at `http://www.sbtoolbox2.org`.

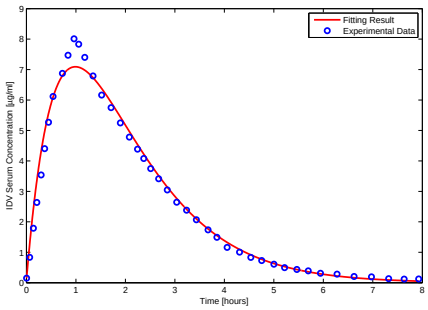

Figure 4.4: Indinavir (IDV) experimental kinetic data fit, for an initial dose of 800 mg.

For 3TC, the fitting obtained is very good, with the simulated data following the experimental data in for all data points. However, for IDV, the fitting does not allow to mimic the plasma concentration peak correctly. This results from the fact that this peak is very sharp for IDV, while it is smoother for 3TC. Still, the fitting correctly predicts the drug kinetic behavior everywhere else.

4.1.2 Drugs Pharmacodynamic Data

For the pharmacodynamic model, only one parameter is needed: C_{50} (see Section 2.3.2). This parameter represents the drug plasma concentration that corresponds to half the maximum effect. In the case of 3TC, this value is 0.73 μM [52], which corresponds to 0.1674 mg/L. For IDV, the value for C_{50} is 0.43μM [53], which corresponds to 0.2639 mg/L[2]. The value used for $E_{\max}$, which corresponds to the maximum drug efficacy (that may range from 0 to 1) is 0.9, to account for the fact that the drug is never 100% effective.

In Figure 4.5 is represented the behavior of the pharmacodynamic model used in this work for each drug, according to (2.3).

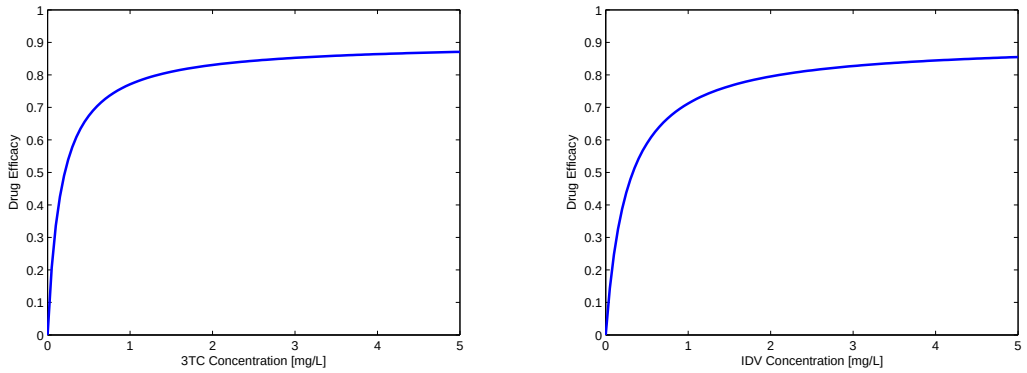

(a) 3TC **(b)** IDV

Figure 4.5: Pharmacodynamic model behavior for both 3TC and IDV.

[2]Molar masses for 3TC and IDV are, respectively, 229.29 g/mol and 613.79 g/mol.

4.2 Numerical Simulations with Drug Action

In this Section, the goal is to analyze how the full model behaves. This full model includes not only the dynamic HIV-1 infection model defined by (2.8) in Section 2.5.2,

$$\begin{cases} \dot{T} &= s - dT - (1-u_1)\beta T\nu \\ \dot{T}^* &= (1-u_1)\beta T\nu - \mu T^* \\ \dot{\nu} &= (1-u_2)kT^* - c\nu \end{cases}, \tag{4.3}$$

but also the pharmacokinetic and pharmacodynamic models (defined by (2.1) and (2.3) in Section 2.3 and further discussed in the previous Section),

$$\dot{\mathbf{x}}(t) = \mathbf{A}\mathbf{x}(t),\ \mathbf{x}(0) = \mathbf{x}_0,\ t \geq 0, \tag{4.4}$$

$$u(C_P) = E_{\max}\frac{C_P}{C_P + C_{50}} \tag{4.5}$$

as well as the adherence and resistance models (in Section 2.4)

$$A = \begin{cases} 1, & \text{if all drug doses are taken by the patient} \\ R_k, & \text{if } 100R_k\% \text{ drug doses are taken by the patient.} \end{cases} \tag{4.6}$$

$$C_{50}(t) = \left(1 + K_R\int_0^t \max\left[0, L_R - C_P(\tau)\right]d\tau\right)C_{50_{base}} \tag{4.7}$$

The parameters used for the drug resistance and pharmacodynamic model are described in Table 4.1.

Table 4.1: Parameters used for the drug resistance model in (2.5)

RTI Concentration Limit L_R	0.001 mg/L
PI Concentration Limit L_R	0.045 mg/L
RTI Resistance Gain K_R	5
PI Resistance Gain K_R	0.5
RTI E_{max}	0.9
PI E_{max}	0.9

4.2.1 Full Model Simulation with 100% Patient Adherence

The first simulation is performed using the standard values for the drug dosage: 300 mg of 3TC every 24 hours, and 800 mg of IDV every 8 hours. As for the patient adherence, it is considered to be 100%, meaning that the patient does not fail to follow the prescription. This simulation is performed to be used as a comparison point for the ones that will follow. Results are shown in Figures 4.6 and 4.7.

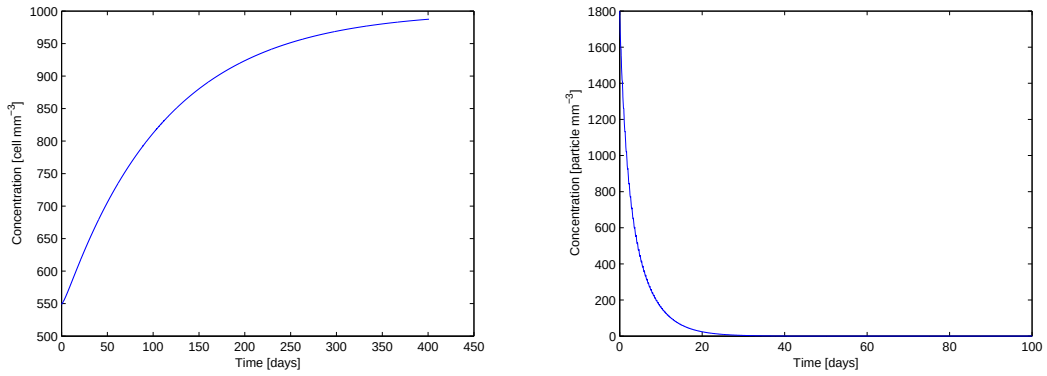

(a) Healthy CD4+ T cells **(b)** Free Virus Particles

Figure 4.6: Dynamic HIV-1 infection full model simulation, including drug effect, considering a patient adherence of 100%. Initial conditions are the HIV-1 dynamic model steady state, which are computed in (2.17).

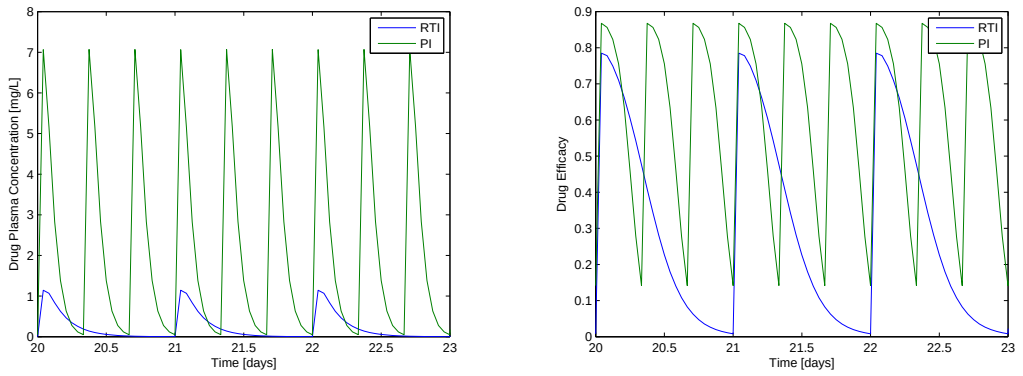

(a) Drug Plasma Concentration **(b)** Drug Efficacy

Figure 4.7: Drug plasma concentration and drug efficacy, for the simulation represented in Figure 4.6.

From this simulation, it is possible to see that the drug dosage used is sufficient to take the viral load to negligible values in a matter of approximately 1 month. However, since the virus load is never 0, if the treatment is suspended, the viral load will increase again, and the healthy CD4+ T cell count will decrease back to the initial endemic steady state. As for the drug plasma concentration, it has a 24-hour period for the RTI and an 8-hour period for the PI, which is expectable given the fact that the RTI is taken every 24 hours and the PI is taken every 8 hours. Moreover, the PI plasma concentration peak is about 7 times as high as the RTI concentration peak. This happens not only due to the higher dose for the PI (800 mg compared to 300 mg), but also because of the different parameters for the pharmacokinetic model that lead to different drug absorption into the blood stream. Finally, the drug efficacies also exhibit the same periods as the plasma concentrations, and the PI efficacy has a higher peak than the RTI (0.87 compared 0.78).

This happens because the peak in plasma concentration for the PI is much higher than the PI C_{50}, therefore bringing the drug efficacy closer to its limit (which is 0.9). However, given the plasma concentration behavior, the PI efficacy also oscillates a lot more, while the RTI efficacy can hold at higher values longer.

4.2.2 Model Simulation with 50% Patient Adherence

One of the main problems with antiretroviral therapy is the lack of patient adherence to the treatment. This results in periods when drug plasma concentration is nearly zero, and consequently, drug efficacy is also zero. Moreover, when drug plasma concentration is low, the virus has the opportunity to develop drug resistance. In this simulation, this effect is explored, by setting the patient adherence to both drugs to 50%, meaning that, in average, only half of the prescribed doses are actually taken. Results are shown in Figures 4.8 and 4.9.

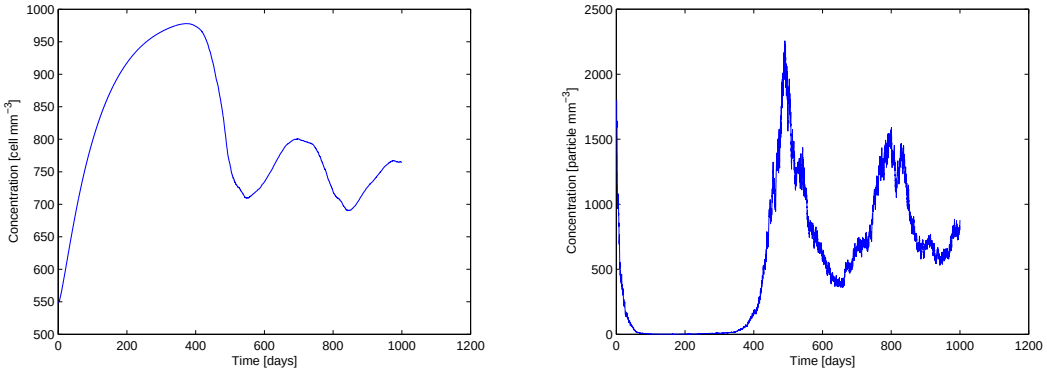

(a) Healthy CD4+ T cells **(b)** Free Virus Particles

Figure 4.8: Dynamic HIV-1 infection full model simulation, considering a patient adherence of 50%.

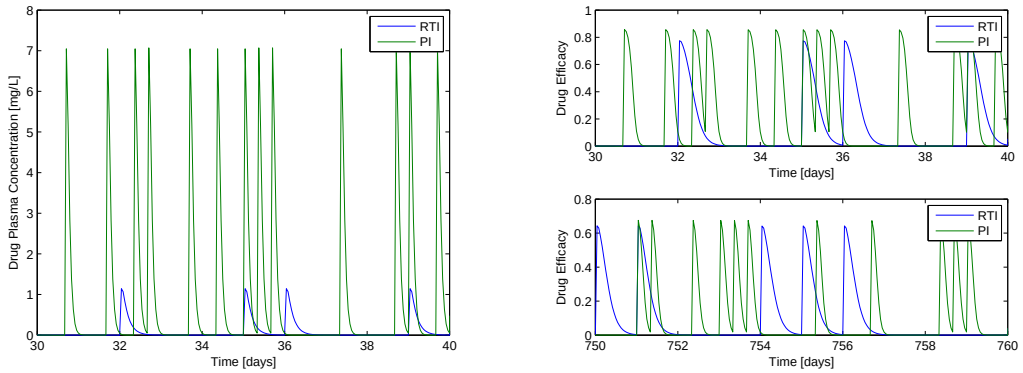

(a) Drug Plasma Concentration **(b)** Drug Efficacy

Figure 4.9: Drug plasma concentration and drug efficacy, for the simulation represented in Figure 4.8.

An immediate conclusion that can be drawn from this simulation is that such a low patient adherence implies that the infection subsides only for a certain amount of time (in this case, about a year). After that, the viral load rises again, and the healthy CD4+ T cell count drops. The explanation for this effect is based on the resistance model used. Because of the low adherence value, there are time periods in which drug plasma concentration is below the threshold value, and therefore the values for values for RTI and PI C_{50} are increased, meaning that the drug efficacies drop to lower values, even when the medication is taken. This can be clearly seen in Figure 4.9(b), where the peak value for the drug efficacies in the first days is around 0.8, while for later stages it is around 0.6-0.7. The accumulation of this effect over time results in therapy failure after approximately one year. Moreover, since the increase in the values for C_{50} is irreversible, it is not possible to control the infection, even if patient adherence is increased after the infection reappears.

4.2.3 Model Simulation with lower drug dosages

Another factor that is very important in the HIV-1 infection treatment outcome is the drug dosage. If the drug doses are not high enough, there are periods in which drug plasma concentration is nearly zero. On the other hand, very high drug doses may lead to undesirable side effects and drug toxicity. The values used in the Sections above are those that are recommended by physicians and that are most suitable for the common infection. In this simulation, the objective is to assess what happens if these dosages are lowered significantly. Therefore, the dosages used are 100 mg of 3TC every 24 hours, and 200 mg of IDV every 8 hours. This means that the RTI dosage is reduced by two thirds, while the PI dosage is reduced by three quarters. To be able to compare the results with those in Section 4.2.1, patient adherence is considered to be 100% in this simulation. Results are shown in Figures 4.10 and 4.11.

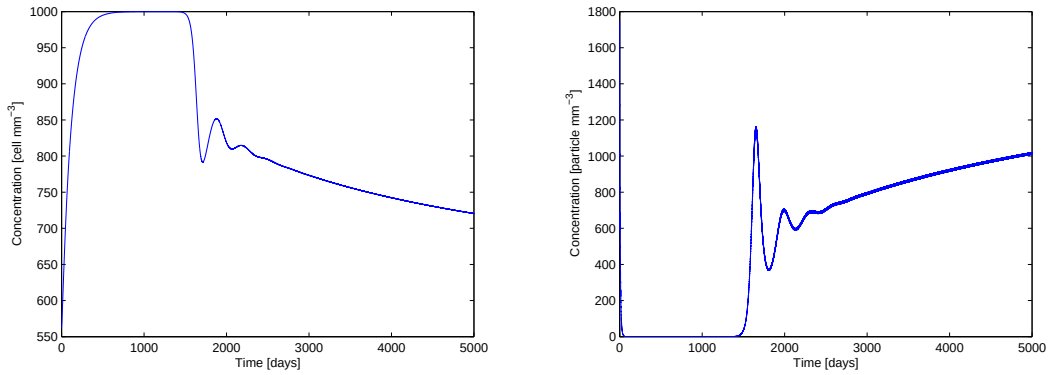

(a) Healthy CD4+ T cells

(b) Free Virus Particles

Figure 4.10: Dynamic HIV-1 infection full model simulation, including drug effect, considering a dosage of 100 mg of 3TC every 24 hours, and 200 mg of IDV every 8 hours, for a patient adherence of 100%.

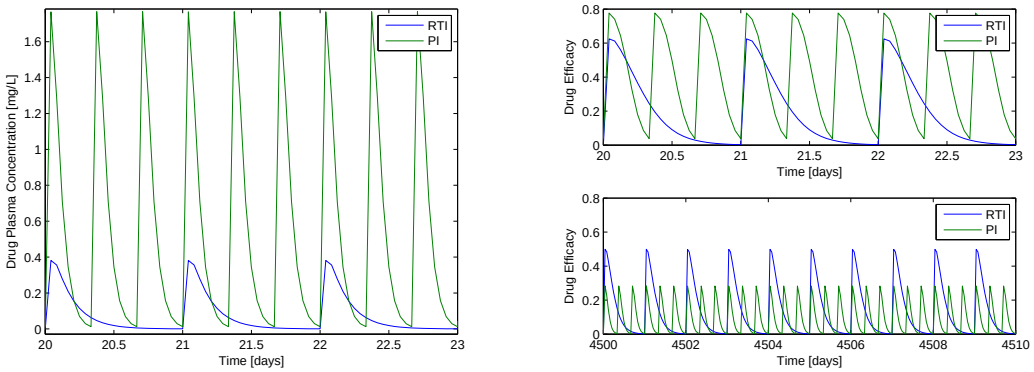

(a) Drug Plasma Concentration

(b) Drug Efficacy

Figure 4.11: Drug plasma concentration and drug efficacy, for the simulation represented in Figure 4.10.

From the results, it can be seen that this drastic reduction in drug dosage is enough to compromise the treatment in the period of 4-5 years. After this period, the infection resurfaces, due to the resistance it developed to the antiretroviral drugs. While in the previous case this resistance was due to lack of patient adherence (which leads to periods when drug concentration was practically zero), in this case the resistance develops because of chronic insufficient drug dosage, that makes the drug plasma concentration to fall below the resistance threshold systematically for short periods.

Given the time necessary for the resistance to present itself in this case as well as in the previous case, it can be concluded that it is better to follow a tight schedule on lower drug dosages than to fail to take the prescribed drugs at higher dosages. This fact is supported by Figure 4.11(b), where it is clear that in later treatment stages (after 12 years), the drug efficacy peaks are still at reasonable values of 0.5 for 3TC and 0.3 for IDV. Even though the simulation in Section 4.2.2 does not go that far in time, it is predictable that, given the decay rate of drug efficacy by the day 750, these values would be much lower by the time the simulation reached 12 years.

4.2.4 Model Simulation with Half Sampling Frequency

This last simulation intends to compare the results obtained in Section 4.2.2 (where patient adherence is 50%), with an equivalent situation, where the drugs are administered to the patient with half the frequency. This means that 300 mg of 3TC are given every 48 hours, while 800 mg of IDV are administered every 16 hours. For the situation to be equivalent to that of Section 4.2.2, patient adherence is considered to be 100% in this simulation. Results are shown in Figures 4.12 and 4.13.

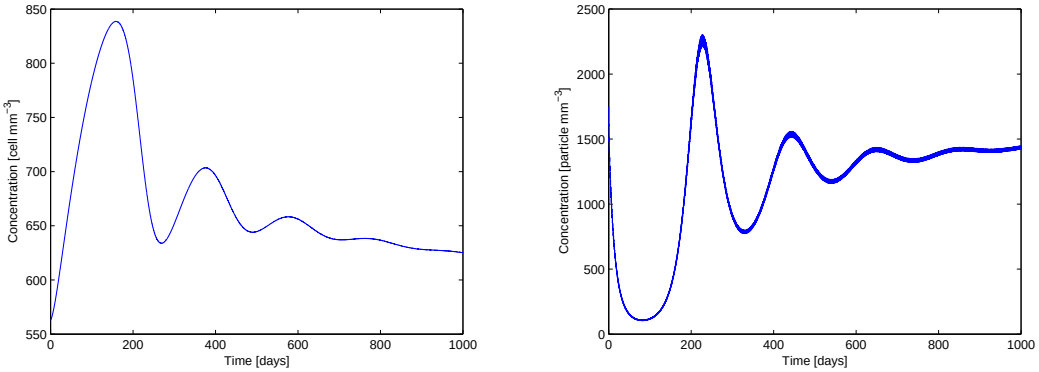

(a) Healthy CD4+ T cells **(b)** Free Virus Particles

Figure 4.12: Dynamic HIV-1 infection full model simulation, including drug effect, with half drug administration frequency.

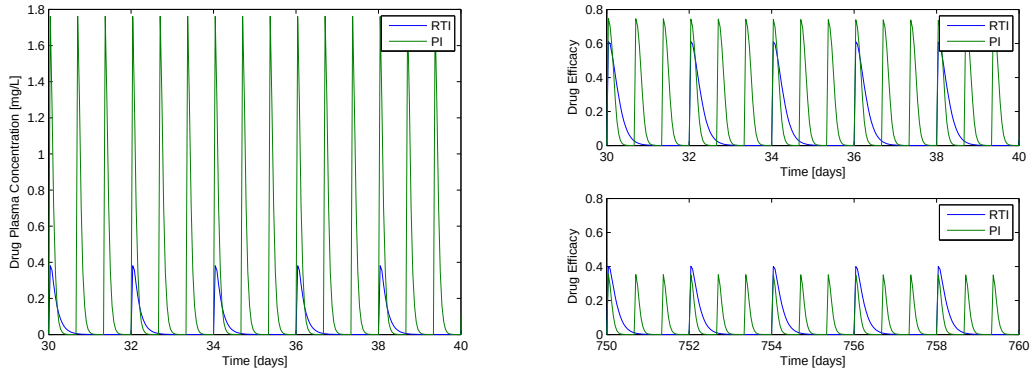

(a) Drug Plasma Concentration **(b)** Drug Efficacy

Figure 4.13: Drug plasma concentration and drug efficacy, for the simulation represented in Figure 4.12.

Comparing the results from Figure 4.8 with those obtained in this simulation, it is clear that in the last case the "almost" healthy state (with viral load close to zero and healthy CD4+ T cell count near 1000) is never achieved. Around day 100, the viral load rebounds, rendering the treatment almost useless. This does not happen in Figure 4.8, where only after about a year the viral load starts to rise and the CD4+ T cell count starts to drop. Therefore, it can be concluded that administering the drugs with half the frequency but with 100% adherence leads to a worse outcome than having a normal therapy with 50% adherence (as simulated in Section 4.2.2). This may be explained in a simple way: if the drugs are administered randomly, there is a high probability that at some point, in the beggining of the treatment, there are a few days where the percentage of doses taken is very high. This means that, even if only for a short period, the virus is correctly suppressed, and is therefore almost eliminated from the system (looking at

Figure 4.6(b) it is possible to see that approximately 30-40 days are enough to set the virus load to approximately zero, when the prescription is followed accurately). Once the virus is at a low level, the amount of drug necessary to keep it that way is smaller, justifying the fact that the random prescription works better. Naturally, the C_{50} of both drugs increases approximately the same in both regimes, which leads to the eventual failure of the treatment.

5

Nonlinear Control of HIV-1 Infection Model

Contents

The final step of this work is to implement a control algorithm that allows to adjust the drug doses, so that patients receive only as much antiretroviral drugs as they need. In the first part of this Chapter, a brief revision over Nonlinear Control theory is presented. After that, results from two different control algorithms (one comprising only drug efficacies, and another considering drug doses as input) are presented and discussed.

5.1 Nonlinear Control

Control is a branch of engineering and mathematics, and consists of a mathematical study of how to manipulate the parameters affecting the behavior of a system to produce the desired or optimal outcome [54]. The main purposes of controlling a system are:

- Maintain the output at a desirable value or reference.
- Stabilize the controlled system.
- Impose a convenient dynamics to the system.
- Optimize the system with respect to a certain quantity (for example, energy consumption), maintaining the objectives.
- Maintain a constant system behavior, even when dynamics change.

For the HIV-1 infection, the system to be controlled is the infection dynamic model presented earlier. This control is performed by a doctor (controller), that may adjust the treatment based on the viral load (sensor), when measurements are performed. This closed-loop mechanism is summarized in Figure 5.1.

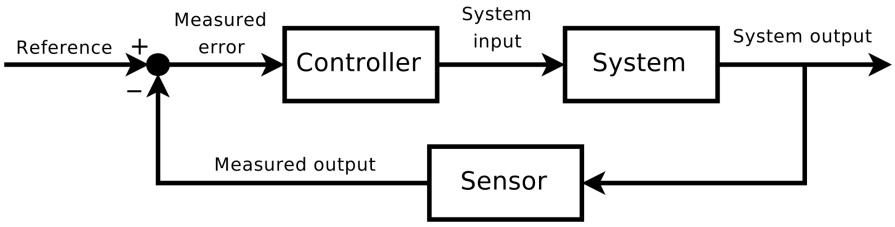

Figure 5.1: Closed-loop feedback of a dynamic system.

The control objective in the case of the HIV-1 infection may not be clear. Naturally, the main concern is always to drive the viral load to the lowest value possible. However, it may also be reasonable to say that a successful treatment is the one that can lead to a regularization of the T cell count, or the one that can achieve the main goal with the least amount of drug, or even the one that minimizes toxicity, and therefore, side-effects.

The first step is, consequently, to define the control objective. The first and main objective is to maintain the viral load ν at a predefined value r. At every iteration (with each iteration

representing one day), the purpose is to minimize the difference between the viral load at the next iteration and r. Additionally, another objective is set, which is to minimize the amount of drug used in the attempt of fulfilling the main objective.

Control is achieved by finding the inputs ($D_1(k)$ and $D_2(k)$) that best fit the objectives presented above. However, at any iteration k, the viral load at the next iteration $(k+1)$ is not know. Therefore, it needs to be estimated as closely as possible. In this work, a simple relation between $\nu(k+1)$, $\nu(k)$, $u_1(k)$ and $u_2(k)$ is used, given by

$$\nu(k+1) = a\nu(k) + b_1 u_1(k) + b_2 u_2(k) \tag{5.1}$$

This expression assumes that viral load is measured everyday, and therefore the viral load in the following day is defined as being proportional to the viral load today, as well as to the drug effects. In order to estimate a, b_1 and b_2, a Recursive Least Squares (RLS) algorithm is used [55] alongside the control algorithm. However, the inputs that the system allows are $D_1(k)$ and $D_2(k)$, while (5.1) uses the drug effects $u_1(k)$ and $u_2(k)$. Because the relationship between $D_i(k)$ and $u_i(k)$ $(i = 1, 2)$ is not simple, an approximation is used. Whenever it is necessary to compute $u_i(k)$, the PK/PD model is simulated for the drug doses $D_i(k)$, and the average drug efficacy $\overline{u}_i(k)$ is computed. Then, it is this value that is used in (5.1), which results in the expression

$$\nu(k+1) = a\nu(k) + b_1 \overline{u}_1(k) + b_2 \overline{u}_2(k) \tag{5.2}$$

In the next Sections, two control implementations and results are explained. First, a control algorithm using only drug efficacies u_i (bypassing drug doses D_i) is shown. After that, a more complete model using drug doses is designed.

5.2 Nonlinear Control Results

5.2.1 Model Control using Drug Efficacies

As it is stated in the previous Section, the main goal of the control algorithm is to drive the viral load to a predefined level. Moreover, the algorithm also takes into account the amount of drug necessary to achieve its objective. Since this algorithm uses drug efficacies instead of drug doses, the cost function at iteration k is given by

$$J(k) = \frac{1}{2}\left[(\nu(k+1) - r)^2 + \rho_1 u_1(k)^2 + \rho_2 u_2(k)^2\right] \tag{5.3}$$

where $\nu(k+1)$ is given by 5.1.

A simulation, using the model proposed in Section 2.5.2, was performed using the following parameters:

$$\mathbf{X}_0 = \begin{bmatrix} 562.5, & 13.125, & 1750 \end{bmatrix}' \tag{5.4}$$

$$\boldsymbol{\theta} = \left[\begin{array}{cccccc} 9, & 0.009, & 4 \times 10^{-6}, & 0.3, & 80, & 0.6 \end{array} \right]' \tag{5.5}$$

$$r = 50; \quad \rho_1 = 1; \quad \rho_2 = 1 \tag{5.6}$$

The evolution of the viral load for this simulation is represented in Figure 5.2.

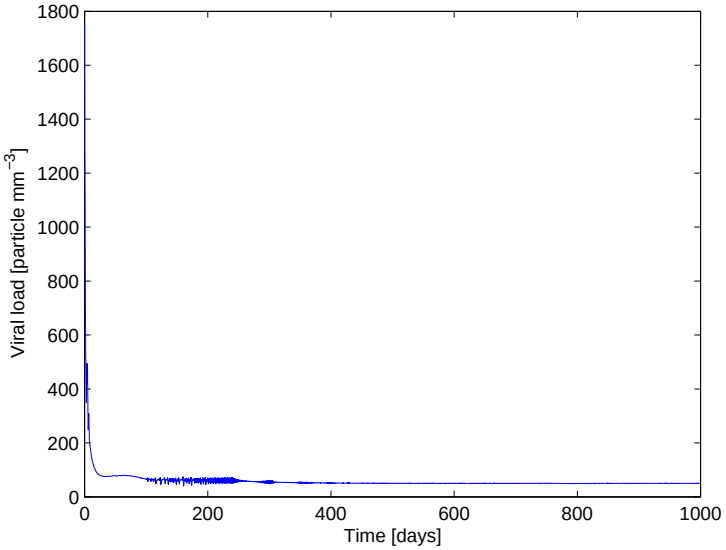

Figure 5.2: Viral load evolution with time, for the control algorithm comprising drug efficacies.

As it is possible to see in Figure 5.2, the viral load quickly drops to 50 copies/ml, and remains at that level for the rest of the simulation. This means that the main control objective is clearly achieved with this algorithm. As to the second objective, this algorithm does not allow to measure the drug doses, since it only uses drug efficacies. Still, the time evolution of the drug efficacies is show in Figure 5.3.

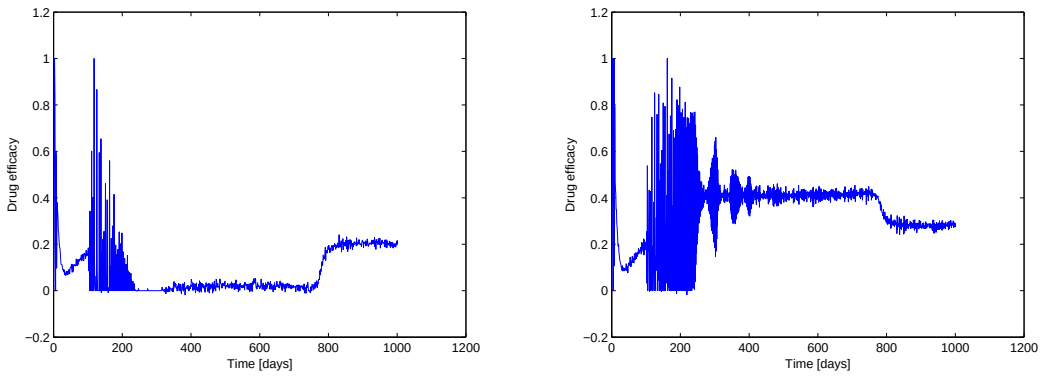

(a) RTI efficacy

(b) PI efficacy

Figure 5.3: Drug efficacy evolution with time, for the control algorithm comprising drug efficacies.

From this results, it can be seen that the drug efficacies are, for the most of the simulation, very low. Even though the efficacies are high in the beginning (when the viral load is still high), they quickly drop once the infection is controlled. This shows that the amount of drugs (or at least their effect) does not need to remain high through the entire treatment. Moreover, it is also evident the two types of drugs are, at least to some extent, complementary and interchangeable. Around day 800, there is a sudden increase in the RTI efficacy, while the PI efficacy decreases. Since the viral load does not change in this period, and these efficacies are the lowest possible that can keep the viral load at the intended level, it can be concluded that it is possible to increase the efficacy (and probably the dose) of one drug and decrease the efficacy of the other, and still expect to maintain the outcome in terms of viral load. This is important because it may allow to reduce the dosage of drugs that are more toxic while increasing the dosage of others that may be less harmful to the human body.

5.2.2 Model Control using Drug Doses

This simulation intends to be an upgrade of the one presented in the previous Section, because it uses drug doses as inputs, rather than drug efficacies. This represents an improvement since it is not possible for a doctor to prescribe drug efficacy. The only available input for the treatment of the HIV-1 infection are the drug doses, and therefore it only makes sense to include them in the control algorithm. Besides, when using drug efficacies, it is not possible to include the PK/PD model and the resistance development model in the simulation, since the work is done directly at the efficacy level.

The control algorithm needs to be adapted to fit this new input variable. Even though the cost function is similar to (5.3), some changes need to be introduced. Using the justification presented in Section 5.1, the cost function used in this algorithm is given by

$$J(k) = \frac{1}{2}\left[(\nu(k+1) - r)^2 + \rho_1 \overline{u}_1(k)^2 + \rho_2 \overline{u}_2(k)^2\right] \tag{5.7}$$

where $\nu(k+1)$ is given by 5.2.

A simulation was performed using the parameters in (5.4), (5.5) and (5.6), where the pharmacokinetic parameters are described in Section 4.1 (Equations (4.1) and (4.2)) and the pharmacodynamic parameters are described in Section 4.1.2. Parameters from Table 4.1 are also used. The patient adherence considered in this simulation was 90%.

The viral load evolution with time is represented in Figure 5.4.

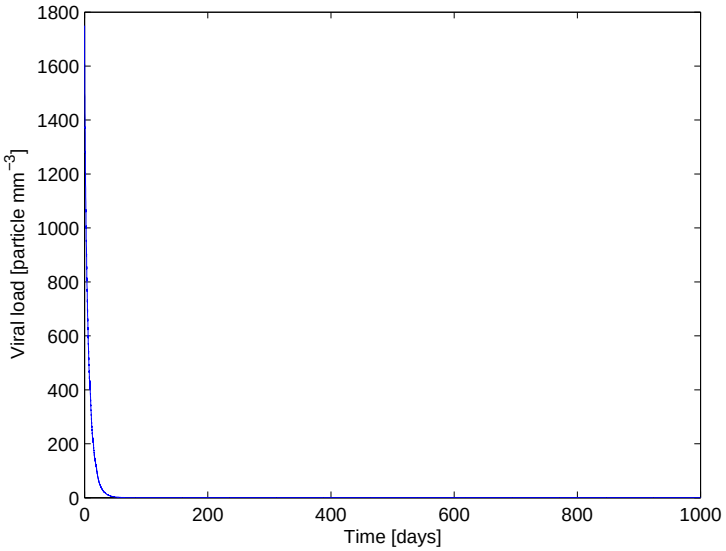

Figure 5.4: Viral load evolution with time, for the control algorithm comprising drug doses.

It is possible to see in Figure 5.2 that, like in the previous simulation, the viral load is quickly controlled, and remains at low levels for the entire simulation, meaning that the main objective is achieved. For the second control objective, it is now possible to assess the amount of drug used in this treatment. These are represented in Figure 5.5.

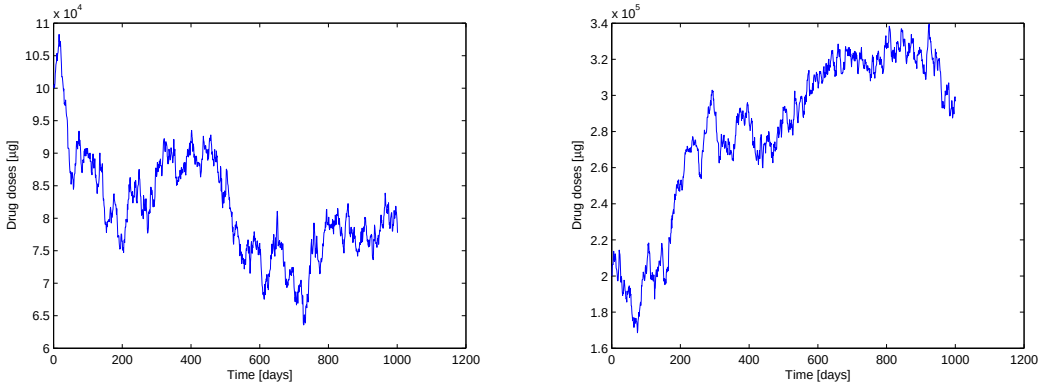

(a) RTI dose **(b)** PI dose

Figure 5.5: Drug doses evolution with time, for the control algorithm comprising drug doses.

Analyzing the results in Figure 5.5, it is possible to see that drug doses as high as 110 mg (for RTI) and 340 mg (for PI) are sufficient to keep the viral load undetectable for the entire simulation. This means that, as it was shown in the previous simulation, drug doses lower than those currently prescribed still maintain high success rates in the infection control. In terms of patient life quality, lower drug doses mean less toxicity and fewer side-effects, which may even lead to an increase in patient adherence to the treatment, rendering it even more effective. These results clearly show

that there is room for improvement in therapy design, in what concerns drug dosage.

However, one fact that this control algorithm does not focus on is the drug plasma concentration not falling below the resistance threshold. In fact, after the simulation is concluded, the values for C_{50}^{RTI} and C_{50}^{PI} are, respectively, 0.2128 mg/L and 0.7467 mg/L (compared to the initial values of 0.1674 mg/L and 0.2639 mg/L). This increase means that resistance is slowly developing due to the low drug doses, which will result in treatment failure eventually. This is expectable, since the cost function does not include any reference to preventing resistance appearance. However, it is possible to see that the control algorithm tries to counteract this effect, through the increase of D_2 over time. The PI dose has a clear tendency of increasing with time, while the RTI dose tends to stay at a stable level. This can be interpreted as an effect of the increase in C_{50}^{PI} (which rises much more than C_{50}^{RTI}). In conclusion, the algorithm shows great potential as a tool for lowering drug dosage without compromising the treatment, but it still needs to be adjusted to take into account the resistance model developed in this work, so that the antiretroviral drugs work equally effectively throughout the entire treatment.

6

Conclusions and Future Work

Contents

6.1 Conclusions

Throughout this dissertation, several conclusions about HIV-1 dynamics can be drawn. The first conclusion obtained is concerned with the comparative study between three different models for the HIV-1 dynamic behavior. It is showed that equilibrium points do not depend on initial conditions, but rather on the parameters used. However, these initial conditions are important to determine the model behavior before the equilibrium is reached. In addition, all three models are consistent with each other, showing alternating peaks of virus particles and CD4+ T cells, until reaching the steady state. The main differences found between the different models considered reside in the extra states added to the simulations. For the model where healthy CD4+ T cell proliferation is considered, the final counts for this population are increased. Moreover, for the model that considers a macrophage cell pool, the viral load final value is also elevated, due to the extra source of cells that can be infected.

From the sensitivity analysis, it can be concluded that, for the studied model, the infection's most informative time period is between the 50^{th} and the 100^{th} day, and that sensitivities quickly drop to negligible values for almost all parameters. After this analysis, a local identifiability study is performed, and a traditional approach (correlation matrix) shows that the HIV-1 infection model is not identifiable. However, the proposed model for the identifiability analysis, based on SVD analysis, shows not only that the model is not identifiable, but also that the unidentifiable parameters are k, s and c.

After the assembly of the full model, considering not only the PK+PD model, but also the adherence and resistance models, several simulations are performed using a therapy composed of two antiretroviral drugs currently available on the market. Analyzing the results from these simulations, the first conclusion that can be reached is that the currently indicated posology is effective in leading the viral load to undetectable values, and maintaining it that way, if patient adherence is 100%. However, if drug dosages are reduced (in the simulations performed, about 30% of the recommended values are used), the therapy fails after approximately 5 years, due to virus resistance. Still, the most conclusive analysis performed was the one in which a model considering 50% adherence was compared with a model with 100% adherence but half the drug administration frequency. From these simulations, it is clear that a patient with 50% adherence can maintain an undetectable viral load for about one year, after which the viral load rebounds due to virus resistance. Nevertheless, this result is far better than that obtained in the other simulation (with half the drug administration frequency). In this case, the viral load is never undetectable, and resistance appears after 100 days. These results are surprising, since the amount of drug administered in both cases are approximately the same. The explanation for this discrepancy lies exactly in the administration randomness, which makes it highly likely that the patient takes the prescribed drugs for a few days correctly. When this happens, the viral load quickly drops to zero, and afterwards, only small amounts of drug are necessary to maintain the viral load undetectable.

The last part of this dissertation consisted in the development of control algorithms that can be applied to the studied HIV-1 dynamic models. Two algorithms are developed, one calculating the drug efficacies necessary to control the infection, and another that computes the drug doses with the same objective. The second algorithm is not only more complex, but also more realistic, since only drug doses can be controlled in real patients. Both algorithms succeed in maintaining the viral load at low levels, while minimizing the amount of drug used. The second algorithm, that considers drug doses, shows that it is possible to control the HIV-1 infection longer than three years with 3TC doses lower than 110mg, and IDV doses lower than 340mg. When compared to the currently recommended posology (300mg and 800mg, respectively), it is possible to conclude that the therapies can be greatly optimized, and drug doses reduced. However, there is one factor that is not considered in these control simulations, and that can influence the results greatly. This factor is the resistance modeling, that is certain to appear eventually and that will lead to therapy failure.

6.2 Future Work

The work developed in this dissertation can still be greatly improved, in what concerns the applicability of these studies to real cases.

Concerning the dynamic model analysis, the proliferation of healthy CD4+ T cells should be included in the proposed model, since this extra term represents a considerable source of T cell production. Moreover, more parameter sets should be used in the comparative study between the three proposed models. The fact that only three models are used in this dissertation is because reliable parameters sets could only be found for these models. Other models, that are considerably more complex, and that have the potential of mimicking the infection dynamics better, should be further investigated.

For the local identifiability analysis there is also margin for improvement. Even though it is concluded that the model is not identifiable and that the least identifiable parameters are k, s and c, no further study is performed in this matter. However, it may be possible to find an identifiable subset of parameters. This can be achieved by fixing the the least identifiable parameter with a reference value, and rerunning the simulation, in order to assess if the model is still not identifiable. This algorithm is repeated until a subset of identifiable parameters is found, or until it is concluded that there are not identifiable parameters.

Further development may also be done in simulations of the full model comprising the PK+PD model as well as the resistance and adherence models. Even though good conclusions are reached in this work, further simulation with different conditions can be done, with the objective of analyzing the differences between therapies. Other drugs can be included in the PK+PD model, so that therapies are more closely related to real cases where cocktails of multiple drugs are used. Therefore, a more complex PD model needs to be developed, in order to compute drug efficacies from multiple

drugs. Moreover, a dependency of the simulation results with patient adherence can also be done, and a critical adherence threshold, below which therapy fails, may be found.

The control algorithms may also be subject to further and more detailed study. Even though good results are achieved, more complex and ambitious cost functions can be developed. In particular, the cost function should reflect some concern with resistance development, so that drug doses prescribed to the patient would be kept at sufficiently high values. In addition, the control algorithm may be changed so that it is possible to say which type of drug should be used the most. Finally, it would also be interesting to change the frequency at which measurements are available. In this work, it is supposed that it is possible to measure the CD4 T cell count and viral load every day. However, in the real case, this is not true, and measurements are often made with an interval of several weeks or months. Therefore, a control algorithm can be developed with the purpose of finding the drug doses that will maintain the desired objective for larger periods.

There is still a wide margin for improvement related to this work, with the primary objective of knowing more about the HIV-1 infection, and even improving the therapies currently available. This work serves as a basis for further research in this field, even though the results obtained are very promising in improving the quality of life of those infected by HIV-1.

Bibliography

[1] F. Gao, E. Bailes, D. L. Robertson, Y. Chen, C. M. Rodenburg, S. F. Michael, L. B. Cummins, L. O. Arthur, M. Peeters, G. M. Shaw, P. M. Sharp, and B. H. Hahn, "Origin of HIV-1 in the chimpanzee *Pan troglodytes troglodytes*," Nature, vol. 397, no. 6718, pp. 436–441, 1999.

[2] M. Lipman, T. Gluck, and M. Johnson, An atlas of differential diagnosis in HIV disease, ser. The Encyclopedia of visual medicine series. Parthenon Pub. Group, 1995.

[3] G. Pantaleo, C. Graziosi, and A. Fauci, "The Immunopathogenesis of Human Immunodeficiency Virus Infection," New England Journal of Medicine, vol. 328, no. 5, pp. 327–335, 1993.

[4] UNAIDS, "UNAIDS Report on the global AIDS epidemic," UNAIDS, Tech. Rep., 2010.

[5] F. J. Palella, K. M. Delaney, A. C. Moorman, M. O. Loveless, J. Fuhrer, G. A. Satten, D. J. Aschman, and S. D. Holmberg, "Declining Morbidity and Mortality among Patients with Advanced Human Immunodeficiency Virus Infection," New England Journal of Medicine, vol. 338, no. 13, pp. 853–860, 1998.

[6] C. Hoffmann and J. Rockstroh, HIV 2010. Medizin Fokus Verlag, 2010.

[7] D. E. Kirschner, A. S. Perelson, and R. Boer, "Dynamics of HIV infection of CD4+ T cells," Mathematical Biosciences, vol. 114, no. 1, pp. 81–125, March 1993.

[8] H. T. Banks, D. M. Bortz, and S. E. Holte, "Incorporation of variability into the modeling of viral delays in HIV infection dynamics." Mathematical biosciences, vol. 183, no. 1, pp. 63–91, May 2003.

[9] D. M. Bortz and P. W. Nelson, "Model selection and mixed-effects modeling of HIV infection dynamics." Bulletin of mathematical biology, vol. 68, no. 8, pp. 2005–2025, November 2006.

[10] D. Commenges, D. Jolly, J. Drylewicz, H. Putter, and R. Thiébaut, "Inference in HIV dynamics models via hierarchical likelihood," Computational Statistics & Data Analysis, vol. 55, no. 1, pp. 446–456, January 2010.

[11] M. Nowak and R. May, Virus dynamics - mathematical principles of imunology and virology. Oxford University Press, 2011.

[12] V. Costanza, P. S. Rivadeneira, F. L. Biafore, and C. E. D'Attellis, "A closed-loop approach to antiretroviral therapies for HIV infection," Biomedical Signal Processing and Control, vol. 4, no. 2, pp. 139–148, April 2009.

[13] P. W. Nelson and A. S. Perelson, "Mathematical analysis of delay differential equation models of HIV-1 infection." Mathematical biosciences, vol. 179, no. 1, pp. 73–94, 2002.

[14] A. S. Perelson, A. U. Neumann, M. Markowitz, J. M. Leonard, and D. D. Ho, "HIV-1 dynamics in vivo: virion clearance rate, infected cell life-span, and viral generation time," Science, vol. 271, no. 5255, pp. 1582–1586, March 1996.

[15] A. Perelson and P. Nelson, "Mathematical Analysis of HIV-1 Dynamics in Vivo," SIAM, vol. 41, no. 1, pp. 3–44, 1999.

[16] D. Wodarz, A. L. Lloyd, V. A. Jansen, and M. A. Nowak, "Dynamics of macrophage and T cell infection by HIV." Journal of theoretical biology, vol. 196, no. 1, pp. 101–113, January 1999.

[17] M. A. Stafford, Y. Cao, D. D. Ho, L. Corey, C. L. Mackall, R. E. Gress, and A. S. Perelson, "Modeling Plasma Virus Concentration and CD4+ T Cell Kinetics during Primary HIV Infection," Journal of Theoretical Biology, vol. 203, no. 3, pp. 285–301, 2000.

[18] P. W. Nelson, J. D. Murray, and A. S. Perelson, "A model of HIV-1 pathogenesis that includes an intracellular delay," AAPS PharmSciTech, pp. 1–30, February 2011.

[19] Y. Huang, S. L. Rosenkranz, and H. Wu, "Modeling HIV dynamics and antiviral response with consideration of time-varying drug exposures, adherence and phenotypic sensitivity," Mathematical Biosciences, vol. 184, no. 2, pp. 165–186, August 2003.

[20] H. Wu, A. A. Ding, and V. De Gruttola, "Estimation of HIV dynamic parameters," Statistics in Medicine, vol. 17, no. 21, pp. 2463–2485, November 1998.

[21] H. Liang, H. Miao, and H. Wu, "Estimation of constant and time-varying dynamic parameters of HIV infection in a nonlinear differential equation model," The annals of applied statistics, vol. 4, no. 1, pp. 460–483, 2010.

[22] X. Xia, "Estimation of HIV/AIDS parameters," Automatica, vol. 39, no. 11, pp. 1983–1988, Nov. 2003.

[23] H. Wu, H. Zhu, H. Miao, and A. S. Perelson, "Parameter identifiability and estimation of HIV/AIDS dynamic models." Bulletin of mathematical biology, vol. 70, no. 3, pp. 785–799, April 2008.

[24] H. Miao, X. Xia, A. S. Perelson, and H. Wu, "On Identifiability of Nonlinear ODE Models and Applications in Viral Dynamics," SIAM Review, vol. 53, no. 1, pp. 3–39, 2011.

[25] J. Guedj, R. Thiébaut, and D. Commenges, "Practical identifiability of HIV dynamics models." Bulletin of mathematical biology, vol. 69, no. 8, pp. 2493–2513, November 2007.

[26] H. Chang and A. Astolfi, "Enhancement of the immune system in HIV dynamics by output feedback." Automatica, vol. 45, no. 7, pp. 1765–1770, 2009.

[27] S. S. Ge, Z. Tian, and T. H. Lee, "Nonlinear control of a dynamic model of HIV-1." IEEE Trans Biomed Eng, vol. 52, no. 3, pp. 353–361, 2005.

[28] M. Barao and J. Lemos, "Nonlinear control of HIV-1 infection with a singular perturbation model," Biomedical Signal Processing And Control, vol. 2, no. 3, pp. 248–257, 2007.

[29] D. Stowell, "The Molecules of HIV - A Hypertextbook," 2006, Accessed 11-August-2011. [Online]. Available: http://www.mcld.co.uk/hiv/

[30] L. Scherer, J. J. Rossi, and M. S. Weinberg, "Progress and prospects: RNA-based therapies for treatment of HIV infection." Gene Therapy, vol. 14, pp. 1057–1064, 2007.

[31] D. C. Chan and P. S. Kim, "HIV Entry and Its Inhibition." Cell, vol. 93, pp. 681–684, May 1998.

[32] S. Ivanchenko, W. J. Godinez, M. Lampe, H. Kräusslich, R. Eils, K. Rohr, C. Bräuchle, B. Müller, and D. C. Lamb, "Dynamics of HIV-1 Assembly and Release," PLoS Pathog, vol. 5, no. 11, p. e1000652, November 2009.

[33] B. Bean, "Antiviral Therapy: Current Concepts and Practices," Clin Microbiol Res, vol. 5, no. 2, pp. 146–182, April 1992.

[34] J. M. Bailey and W. M. Haddad, "Drug dosing control in clinical pharmacology," Control Systems, IEEE, vol. 25, no. 2, pp. 35 – 51, april 2005.

[35] Y. Huang, D. Liu, and H. Wu, "Hierarchical Bayesian methods for estimation of parameters in a longitudinal HIV dynamic system," Biometrics, vol. 62, no. 2, pp. 413–423, July 2006.

[36] J. Pinheiro, J. M. Lemos, and S. Vinga, "Nonlinear MPC of HIV-1 infection with periodic inputs," in 50th IEEE Conference on Decision and Control and European Control Conference, to be held in Orlando, FL, USA, December 2011.

[37] A. C. Guyton and J. E. Hall, Textbook of Medical Physiology. Elsevier Saunders, 2006.

[38] I. K. Craig, X. Xia, and J. W. Venter, "Introducing HIV/AIDS Education Into the Electrical Engineering Curriculum at the University of Pretoria," IEEE Transactions on Education, vol. 47, no. 1, pp. 65–73, February 2004.

[39] I. Craig and X. Xia, "Can HIV/AIDS be controlled? Applying control engineering concepts outside traditional fields," Control Systems, IEEE, vol. 25, no. 1, pp. 80–83, February 2005.

[40] E. T. Chiyaka, G. Magombedze, and L. Mutimbu, "Modelling within Host Parasite Dynamics of Schistosomiasis." Computational and Mathematical Methods in Medicine, vol. 11, no. 3, pp. 255–280, 2010.

[41] T. M. Apostol, Cálculo. Editora reverté, 1994, no. v. 1.

[42] S.Vinga, K.Thomaseth, J.M.Lemos, A.R.Neves, H.Santos, and A.T.Freitas, "Structural analysis of metabolic networks: A case study on *Lactococcus lactis*," in CONTROLO 2008, 8th Portuguese Conference on Automatic Control, July 2008, pp. 566 – 571.

[43] J. A. Jacquez and T. Perry, "Parameter estimation: local identifiability of parameters." The American journal of physiology, vol. 258, no. 4 Pt 1, pp. E727–E736, April 1990.

[44] J. A. Jacquez and P. Greif, "Numerical parameter identifiability and estimability: Integrating identifiability, estimability, and optimal sampling design," Mathematical Biosciences, vol. 77, no. 1-2, pp. 201 – 227, 1985.

[45] D. E. Zak, G. E. Gonye, J. S. Schwaber, and F. J. Doyle, "Importance of input perturbations and stochastic gene expression in the reverse engineering of genetic regulatory networks: insights from an identifiability analysis of an in silico network," Genome Research, vol. 13, no. 11, pp. 2396–2405, 2003.

[46] G. Golub and W. Kahan, "Calculating the Singular Values and Pseudo-Inverse of a Matrix," Journal of the Society for Industrial and Applied Mathematics: Series B, Numerical Analysis, vol. 2, no. 2, pp. 205–224, 1965.

[47] Y. Huang, "Long-term HIV dynamic models incorporating drug adherence and resistance to treatment for prediction of virological responses," Computational Statistics & Data Analysis, vol. 52, no. 7, pp. 3765–3778, March 2008.

[48] A. Lopes, C. Martins, J. Cruz, L. Mendão, M. Ventura, M. Farinha, Campos, P. Rocha, and R. Lucas, Boas Práticas de Farmácia Hospitalar - no âmbito da Infecção VIH/SIDA. Coordenação Nacional para a Infecção VIH/SIDA, 2008.

[49] J. P. Sabo, M. J. Lamson, G. Leitz, C. Yong, and T. R. MacGregor, "Pharmacokinetics of nevirapine and lamivudine in patients with HIV-1 infection," Aaps Pharmsci, vol. 2, no. 1, p. E1, 2000.

[50] D. M. Burger, A. M. van Rossum, P. W. Hugen, M. H. Suur, N. G. Hartwig, S. P. Geelen, H. J. Scherpbier, R. M. Hoetelmans, A. G. Vulto, and R. de Groot, "Pharmacokinetics of the Protease Inhibitor Indinavir in Human Immunodeficiency Virus Type 1-Infected Children," Antimicrob Agents Chemother, vol. 45, no. 3, pp. 701–5, 2001.

[51] J. Kennedy and R. Eberhart, "Particle swarm optimization," in Neural Networks IEEE International Conference on, vol. 4, 1995, pp. 1942–1948.

[52] M. Carten and H. Kessler, "Zidovudine, Lamivudine, and Abacavir," in Reverse Transcriptase Inhibitors in HIV/AIDS Therapy, ser. Infectious Disease, V. St.Georgiev, G. Skowron, R. Ogden, and J. M. A. Lange, Eds. Humana Press, 2006, pp. 33–76.

[53] G. C. Williams and P. J. Sinko, "Oral absorption of the HIV protease inhibitors: a current update," Advanced Drug Delivery Reviews, vol. 39, no. 1-3, pp. 211–238, 1999.

[54] J. Zabczyk, Mathematical Control Theory: An Introduction, ser. Modern Birkhäuser Classics. Birkhäuser, 2007.

[55] M. H. Hayes, Statistical Digital Signal Processing and Modeling. John Wiley & Sons, 1996.

A

List of Antiretroviral Drugs for HIV-1

In this Appendix, a comprehensive list of commercially available antiretroviral drugs used to treat HIV-1 infection is presented.

Table A.1: List of Nucleoside analog Reverse Transcriptase Inhibitors.

Drug Name	Short Name	Commercial Name	Manufacturer
Abacavir	ABC	Ziagen®	GSK
Didanosine	ddl	Videx®	BMS
Emtricitabine	FTC	Emtriva®	Gilead Sciences
Stavudine	D4T	Zerit®	BMS
Lamivudine	3TC	Epivir®	GSK
Zidovudine	ZDV	Retrovir®	GSK

Table A.2: List of Nucleotide analog Reverse Transcriptase Inhibitors.

Drug Name	Short Name	Commercial Name	Manufacturer
Tenofovir	TDF	Viread®	Gilead Sciences

Table A.3: List of non-Nucleoside Reverse Transcriptase Inhibitors.

Drug Name	Short Name	Commercial Name	Manufacturer
Efavirenz	EFV	Stocrin®	Merck Sharp & Dohme
Etravirine (TMC-125)	-	-	Janssen-Cilag
Nevirapine	NVP	Viramune®	GMBH

Table A.4: List of associations of Reverse Transcriptase Inhibitors.

Short Name	Commercial Name	Manufacturer
3TC + ZDV	Combivir®	GSK
ABC + 3TC	Kivexa®	GSK
ABC + 3TC + ZDV	Trizivir®	GSK
FTC + TDF	Truvada®	Gilead Sciences
EFV + FTC + TDF	Atripla®	-

Table A.5: List of Protease Inhibitors.

Drug Name	Short Name	Commercial Name	Manufacturer
Atazanavir	ATV	Reyataz®	BMS
Darunavir	DRV	Presista®	Janssen-Cilag
Fosamprenavir	fAPV	Telzir®	GSK
Indinavir	IDV	Crixivan®	Merck Sharp & Dohme
Lopinavir	LPV	Kaletra®	Abbott
Nelfinavir	NFV	Viracept®	Roche
Ritonavir	RTV	Norvir®	Abbott
Saquinavir	SQV	Invirase®	Roche
Tipranavir	TPV	Aptivus®	GMBH

Table A.6: List of Entry Inhibitors.

Drug Name	Short Name	Commercial Name	Manufacturer
Enfuvirtida	ENF	Fuzeon®	Roche
Maraviroc	MVC	Celsentri®	Pfizer
Vicriviroc	VCV	-	Schering-Plough

Table A.7: List of Integrase Inhibitors.

Drug Name	Short Name	Commercial Name	Manufacturer
Elvitegravir	-	-	Gilead-Sciences
Raltegravir	RGV	Isentress®	Merck Sharp & Dohme

B

Steady State Computation

B.1 HIV-1 Original Model Steady State Computation

The original HIV-1 infection dynamic model, without drug effect, is given by

$$\mathbf{f}(\mathbf{X},\boldsymbol{\theta}) = \begin{cases} \dot{T} &= s - dT - \beta T\nu \\ \dot{T}^* &= \beta T\nu - \mu T^* \\ \dot{\nu} &= kT^* - c\nu \end{cases} \tag{B.1}$$

To find the model steady state, it is necessary to compute $\mathbf{f}(\mathbf{X},\boldsymbol{\theta}) = \mathbf{0}$. From the first two states, it is possible to obtain

$$s - dT_{\text{eq}} = \mu T^*_{\text{eq}} \Leftrightarrow T^*_{\text{eq}} = \frac{s - dT_{\text{eq}}}{\mu} \tag{B.2}$$

Then, from the last state, it can be said that

$$kT^*_{\text{eq}} = c\nu_{\text{eq}} \Leftrightarrow T^*_{\text{eq}} = \frac{c\nu_{\text{eq}}}{k} \tag{B.3}$$

Combining (B.2) and (B.3),

$$\frac{c\nu_{\text{eq}}}{k} = \frac{s - dT_{\text{eq}}}{\mu} \Leftrightarrow T_{\text{eq}} = \frac{ks - c\mu\nu_{\text{eq}}}{kd} \tag{B.4}$$

Now, substituting (B.3) and (B.4) into the second state in (B.1), we obtain

$$\left[\frac{ks - c\mu\nu_{\text{eq}}}{kd}\beta - \frac{\mu c}{k}\right]\nu_{\text{eq}} = 0 \tag{B.5}$$

Solving (B.5) for ν_{eq},

$$\nu_{\text{eq}} = 0 \vee \nu_{\text{eq}} = \frac{sk}{\mu c} - \frac{d}{\beta} \tag{B.6}$$

substituting (B.6) into (B.3) and (B.4), the steady states for T and T^* can be obtained.

$$\begin{aligned} \nu_{\text{eq}} = 0 \quad &\Rightarrow \quad T^*_{\text{eq}} = 0 \quad \wedge \quad T_{\text{eq}} = \frac{s}{d} \\ \nu_{\text{eq}} = \frac{sk}{\mu c} - \frac{d}{\beta} \quad &\Rightarrow \quad T^*_{\text{eq}} = \frac{s}{\mu} - \frac{dc}{\beta k} \quad \wedge \quad T_{\text{eq}} = \frac{\mu c}{\beta k} \end{aligned} \tag{B.7}$$

In conclusion, there are two steady stated for the model in (B.1), given by

$$\begin{aligned} T_{\text{eq}} = \frac{s}{d};\ T^*_{\text{eq}} = 0;\ \nu_{\text{eq}} = 0 \\ T_{\text{eq}} = \frac{\mu c}{\beta k};\ T^*_{\text{eq}} = \frac{s}{\mu} - \frac{dc}{\beta k};\ \nu_{\text{eq}} = \frac{sk}{\mu c} - \frac{d}{\beta} \end{aligned} \tag{B.8}$$

B.2 HIV-1 T Cell Proliferative Model Steady State Computation

The HIV-1 infection dynamic model that considers CD4+ T cell proliferation, without drug effect, is given by

$$\mathbf{f}(\mathbf{X},\boldsymbol{\theta}) = \begin{cases} \dot{T} &= s - dT + rT\left(1 - \frac{T+L+T^*}{T_{\max}}\right) - \beta T\nu \\ \dot{L} &= \beta T\nu - dL - \beta_L L \\ \dot{T}^* &= \beta_L L - \mu T^* \\ \dot{\nu} &= kT^* - c\nu \end{cases} \tag{B.9}$$

To find the model steady state, it is necessary to compute $\mathbf{f}(\mathbf{X},\boldsymbol{\theta}) = \mathbf{0}$. From the last state, it is possible to obtain

$$kT^*_{\text{eq}} = c\nu_{\text{eq}} \Leftrightarrow T^*_{\text{eq}} = \frac{c\nu_{\text{eq}}}{k} \tag{B.10}$$

Moreover, from the third state, using the relation in (B.10), it is possible to compute

$$\beta_L L_{\text{eq}} = \frac{\mu c\nu_{\text{eq}}}{k} \Leftrightarrow L_{\text{eq}} = \frac{\mu c\nu_{\text{eq}}}{\beta_L k} \tag{B.11}$$

Now, substituting (B.11) into the second state of (B.9), it follows that

$$\left[\beta T_{\text{eq}} - (d+\beta_L)\frac{\mu c}{\beta_L k}\right]\nu_{\text{eq}} = 0 \Leftrightarrow \nu_{\text{eq}} = 0 \vee T_{\text{eq}} = \frac{(d+\beta_L)\mu c}{\beta_L k\beta} \tag{B.12}$$

If $\nu_{\text{eq}} = 0$, it follows that

$$L_{\text{eq}} = 0 \wedge T^*_{\text{eq}} = 0 \wedge s - dT_{\text{eq}} + rT_{\text{eq}}\left(1 - \frac{T_{\text{eq}}}{T_{\max}}\right) = 0 \Leftrightarrow T_{\text{eq}} = \frac{T_{\max}}{2r}\left(r - d + \sqrt{(r-d)^2 + \frac{4rs}{T_{\max}}}\right) \tag{B.13}$$

On the other hand, using (B.10), (B.11) and $T_{\text{eq}} = \frac{(d+\beta_L)\mu c}{\beta_L k\beta}$, it follows from the first state of (B.9) that

$$\nu_{\text{eq}} = \frac{k\beta_L\left(T_{\max}s + (r-d)T_{\max}T_{\text{eq}} - rT^2_{\text{eq}}\right)}{k\beta_L\left(\beta T_{\max} + r\mu c + \beta_L rc\right)T_{\text{eq}}} \tag{B.14}$$

In conclusion, the two steady states of (B.9) are given by

$$\begin{gathered} T_{\text{eq}} = \frac{T_{\max}}{2r}\left(r - d + \sqrt{(r-d)^2 + \frac{4rs}{T_{\max}}}\right);\ L_{\text{eq}} = 0;\ T^*_{\text{eq}} = 0;\ \nu_{\text{eq}} = 0 \\ T_{\text{eq}} = \frac{(d+\beta_L)\mu c}{\beta_L k\beta};\ \nu_{\text{eq}} = \frac{k\beta_L\left(T_{\max}s + (r-d)T_{\max}T_{\text{eq}} - rT^2_{\text{eq}}\right)}{(k\beta_L\beta T_{\max} + r\mu c + \beta_L rc)T_{\text{eq}}};\ L_{\text{eq}} = \frac{\mu c\nu_{\text{eq}}}{\beta_L k};\ T^*_{\text{eq}} = \frac{c\nu_{\text{eq}}}{k} \end{gathered} \tag{B.15}$$

B.3 HIV-1 Macrophage Model Steady State Computation

The HIV-1 infection dynamic model that considers a macrophage population, without drug effect, is given by

$$\mathbf{f}(\mathbf{X},\boldsymbol{\theta}) = \begin{cases} \dot{T} &= s - dT - \beta T\nu \\ \dot{T}^* &= \beta T\nu - \mu T^* \\ \dot{M} &= s_M - d_M M - \beta_M M\nu \\ \dot{M}^* &= \beta_M M\nu - \mu_M M^* \\ \dot{\nu} &= kT^* + k_M M^* - c\nu \end{cases} \tag{B.16}$$

To find the model steady state, it is necessary to compute $\mathbf{f}(\mathbf{X}, \boldsymbol{\theta}) = \mathbf{0}$. From the third state, it is possible to obtain

$$s_M = (d_M + \beta_M \nu_{\text{eq}}) M_{\text{eq}} \Leftrightarrow M_{\text{eq}} = \frac{s_M}{d_M + \beta_M \nu_{\text{eq}}} \tag{B.17}$$

Substituting (B.17) into the fourth state of (B.16), it follows that

$$\frac{s_M \beta_M \nu_{\text{eq}}}{d_M + \beta_M \nu_{\text{eq}}} = \mu_M M^*_{\text{eq}} \Leftrightarrow M^*_{\text{eq}} = \frac{s_M \beta_M \nu_{\text{eq}}}{\mu_M (d_M + \beta_M \nu_{\text{eq}})} \tag{B.18}$$

Now, from the first state of (B.16), it can be deduces that

$$s = (d + \beta \nu_{\text{eq}}) T_{\text{eq}} \Leftrightarrow T_{\text{eq}} = \frac{s}{d + \beta \nu_{\text{eq}}} \tag{B.19}$$

Substituting (B.19) into the second state of (B.16), it follows that

$$\frac{s \beta \nu_{\text{eq}}}{d + \beta \nu_{\text{eq}}} = \mu T^*_{\text{eq}} \Leftrightarrow T^*_{\text{eq}} = \frac{s \beta \nu_{\text{eq}}}{\mu (d + \beta \nu_{\text{eq}})} \tag{B.20}$$

Finally, substituting ((B.18)) and (B.20) into the last state of (B.16), the steady state for the viral load may be found.

$$\left(\frac{k \beta s}{\mu (d + \beta \nu_{\text{eq}})} + \frac{k_M \beta_M s_M}{\mu_M (d_M + \beta_M \nu_{\text{eq}})} - c \right) \nu_{\text{eq}} = 0 \tag{B.21}$$

The first solution for (B.21) is given by $\nu_{\text{eq}} = 0$. This results in the steady state

$$T_{\text{eq}} = \frac{s}{d};\ T^*_{\text{eq}} = 0;\ M_{\text{eq}} = \frac{s_M}{d_M};\ M^*_{\text{eq}} = 0;\ \nu_{\text{eq}} = 0 \tag{B.22}$$

The other solution for (B.21) is not quite as simple, and therefore only the final result is shown here.

$$\begin{aligned} \nu_{\text{eq}} \quad = \quad & \frac{-\beta_M c d \mu \mu_M - \beta c d_M \mu \mu_M + \beta \beta_M k \mu_M s + \beta \beta_M k_M \mu s_M}{2 \beta b_M c \mu \mu_M} + \\ & + \frac{\sqrt{4 \beta \beta_M c \mu \mu_M (\beta_M d k_M \mu s_M + \beta d_M k \mu_M s - c d d_M \mu \mu_M) + (b c d_M \mu \mu_M + \beta_M (c d \mu \mu_M - \beta (k \mu_M s + k_M \mu s_M)))^2}}{2 \beta b_M c \mu \mu_M} \end{aligned} \tag{B.23}$$

The remaining states equilibrium points can be computed using (B.17), (B.18), (B.19) and (B.20)